



An Assessment of the Magmatic Conditions of Late Neoproterozoic Collisional and Post-collisional Granites From the Guéra Massif, South-Central Chad

Chi Thi Pham¹, J. Gregory Shellnutt^{1*}, Meng-Wan Yeh¹ and Yoshiyuki Iizuka²

¹ Department of Earth Sciences, National Taiwan Normal University, Taipei, Taiwan, ² Institute of Earth Sciences, Academia Sinica, Taipei, Taiwan

OPEN ACCESS

Edited by:

Scott Andrew Whattam,
King Fahd University of Petroleum
and Minerals, Saudi Arabia

Reviewed by:

Kenneth Johnson,
University of Houston–Downtown,
United States
Marcos Garcia-Arias,
University of Los Andes, Colombia

*Correspondence:

J. Gregory Shellnutt
jgshelln@ntnu.edu.tw

Specialty section:

This article was submitted to
Petrology,
a section of the journal
Frontiers in Earth Science

Received: 14 February 2020

Accepted: 06 July 2020

Published: 04 August 2020

Citation:

Pham CT, Shellnutt JG, Yeh M-W
and Iizuka Y (2020) An Assessment
of the Magmatic Conditions of Late
Neoproterozoic Collisional
and Post-collisional Granites From
the Guéra Massif, South-Central
Chad. *Front. Earth Sci.* 8:318.
doi: 10.3389/feart.2020.00318

The Guéra Massif, in South-Central Chad hosts granitic rocks that were emplaced during distinct intervals (595–590; ~570; ~560 Ma) of the Late Ediacaran Central African Orogenic Belt. To the northwest of the Guéra Massif, younger post-collisional granites (554–545 Ma) are found near Lake Fitri. The older (≥ 590 Ma) rocks have geochemical characteristics of collisional granites whereas the younger (≤ 570 Ma) rocks are similar to post-collisional granites. Biotite and amphibole were analyzed to constrain the magmatic conditions of the granites. The biotite from the collisional granites tends to have higher Al and Ti and lower Fe# (Fe#_{average} ≈ 0.67) than the post-collisional granites (Fe#_{average} ≈ 0.88). The average crystallization temperatures range from 696 ± 37 to $612 \pm 8^\circ\text{C}$, with the average pressure of crystallization from 0.25 ± 0.09 to 0.13 ± 0.02 GPa, and redox conditions between the nickel-nickel oxide (NNO) and quartz-fayalite-magnetite (QFM) buffers. The biotite crystallization temperatures of the post-collisional rocks are generally lower than the collisional rocks (570 Ma = 630 ± 26 to $619 \pm 30^\circ\text{C}$, 560 Ma = 626 ± 20 to $607 \pm 4^\circ\text{C}$, 550 Ma = 639 ± 18 to $612 \pm 13^\circ\text{C}$), but the crystallization pressures are similar (0.27 ± 0.05 to 0.14 ± 0.04 GPa). The redox conditions transition from the QFM buffer to the wüstite-magnetite (WM) buffer. In contrast, the biotite from the Lake Fitri post-collisional granites crystallized at higher pressure (0.39 ± 0.08 to 0.35 ± 0.03 GPa) but similar redox conditions. The amphiboles in the younger (~590 Ma) collisional granites and the post-collisional granites yielded crystallization pressure estimates that are generally higher (~0.6 to 0.1 GPa) than the biotite estimates but there is overlap. The difference in pressure may be due to the timing of crystallization and/or crystal redistribution. Overall, there appears to be a secular change from high to low temperature and pressure whereas the redox conditions appear to be spatially related. The biotite crystallization pressure of the Lake Fitri granites suggests they were likely emplaced into a different domain/terrane of the Saharan Metacraton than the Guéra Massif.

Keywords: Saharan Metacraton, biotite chemistry, Guéra Massif, collisional granites, post-collisional granite, Central African Orogenic Belt

INTRODUCTION

The Saharan Metacraton occupies the North-Central part of Africa and covers an area of ~ 5 million km² (Abdelsalam et al., 2002; Liégeois et al., 2013). It is surrounded by the Tuareg Shield to the west, the Arabian-Nubian Shield (ANS) to the east, the Congo Craton to the south, and the African continental margin to the north (**Figure 1A**). The boundaries of the Saharan Metacraton are the result of lithospheric-scale suturing processes caused by Neoproterozoic (~ 750 – 550 Ma) collisional events. The eastern boundary is considered to be the north-trending Keraf–Kabus–Sekerr Shear Zone which is an arc-continental suture that separates the Saharan Metacraton from the ANS (Abdelsalam and Dawoud, 1991; Stern, 1994; Abdelsalam and Stern, 1996). The western boundary is the north-trending Raghane Shear Zone which marks the collision zone between the Saharan Metacraton and the Tuareg Shield (Liégeois et al., 1994, 2003; Henry et al., 2009). The southern boundary is not well-defined but is considered to be the northern border of the Central African Orogenic Belt (CAOB) in the southwest and the Aswa Shear Zone farther east. The east-west trending CAOB separates the Saharan Metacraton from the Congo Craton to the south (Pin and Poidevin, 1987; Poidevin, 1994; Toteu et al., 2006). The northern boundary of the Saharan Metacraton is unconstrained but is likely located in southern Egypt and Libya and covered by thick Phanerozoic sediments (Abdelsalam et al., 2002).

The Saharan Metacraton comprises medium to high-grade metamorphic rocks including gneiss, metasedimentary rocks, migmatites and granulites as well as low-grade volcano-sedimentary sequences that are intruded by Neoproterozoic granitic rocks (Klerkx and Deutsch, 1977; Stern et al., 1994; Sultan et al., 1994; Abdelsalam et al., 2002; Shang et al., 2010). Isotope model ages and U-Pb geochronology of basement rocks vary from ~ 3100 to 500 Ma suggesting there is an Archean ancestry within the Saharan Metacraton (Abdelsalam et al., 2002). Nevertheless, the principal magmatic phases of the Saharan Metacraton occurred from ~ 750 to 550 Ma (Abdelsalam et al., 2002; Suayah et al., 2006; Shellnutt et al., 2017, 2018).

Mesoproterozoic to Neoproterozoic rocks of the Saharan Metacraton are exposed in Chad within the Tibesti, Ouaddaï, and Guéra massifs (**Figure 1B**). The Guéra Massif is located in South-Central Chad and is primarily comprised of granitic rocks many of which are cross-cut by dolerite dykes (Isseini et al., 2013; Nkouandou et al., 2017). The main lithologic and structural characteristics are described by Isseini et al. (2013), and the geochronology and geochemistry are documented by Pham (2018). Granitic intrusions were emplaced during and after the collision between the Congo-São Francisco Craton and the Saharan Metacraton. Pham (2018) proposed that there are two types of granites: (1) the older (595–590 Ma), collision-related granites that formed by subduction and syn-collisional processes, and (2) the younger (570–560 Ma), post-collisional granites. Furthermore, even younger (554–545 Ma) post-collisional granites are located ~ 150 to 350 km to the NW of the Guéra Massif near Lake Fitri and are compositionally similar to the Guéra post-collisional granites. Consequently, the Lake Fitri granites could be representative of a third post-collisional

period in south-central Chad, and/or represent a northwestward extension of the Guéra Massif (**Figures 1C,D**; Shellnutt et al., 2017, 2018).

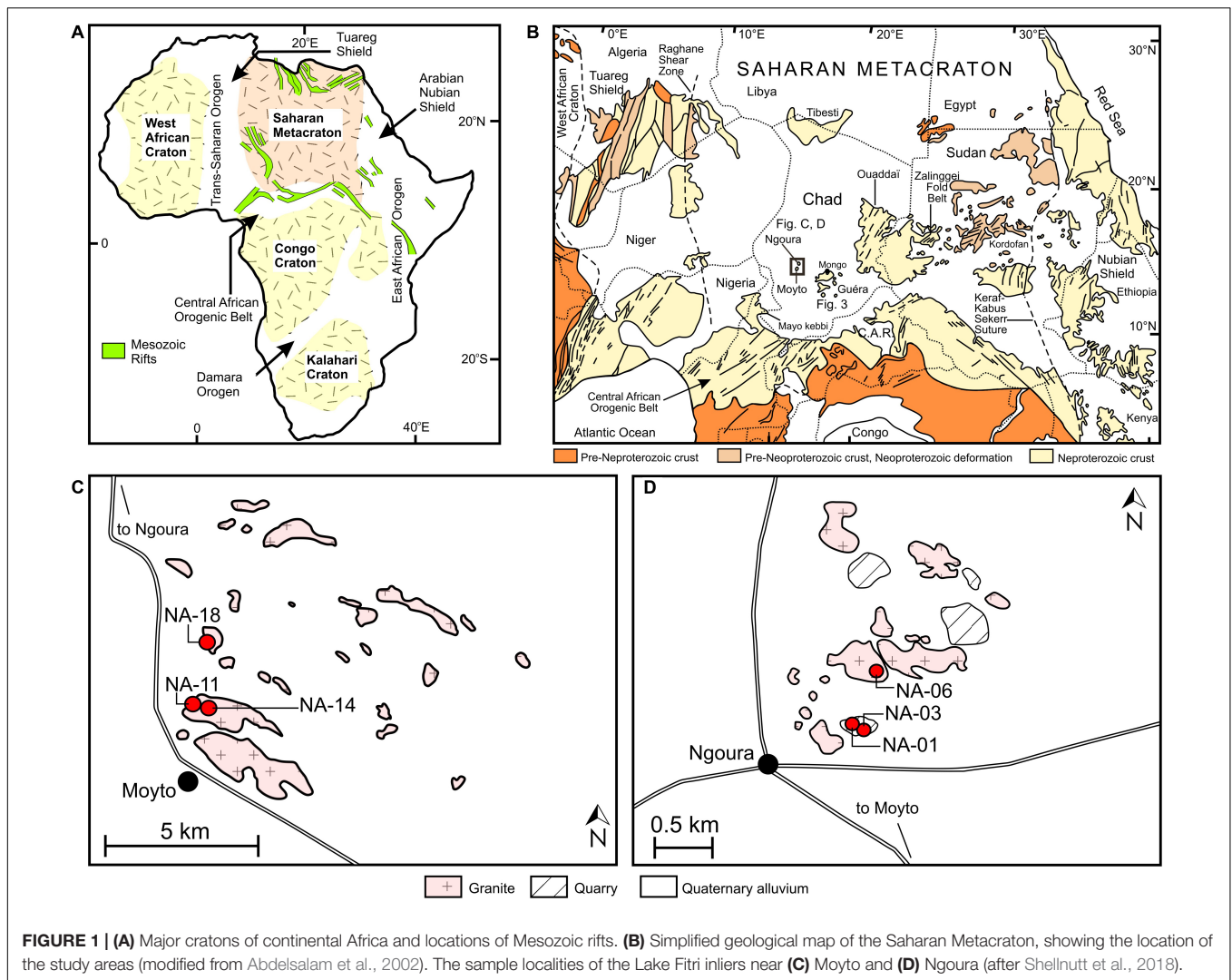
Mafic minerals (e.g., amphibole, biotite) are fundamental components of many granitic rocks. For example, the compositions of amphibole and biotite reflect the magmatic conditions and the nature of the parental magma from which they crystallized (Zen, 1988; Abdel-Rahman, 1994; Shabani et al., 2003). In general, biotite composition can be used to: (1) track the oxidation state of the melt from which it crystallized (Wones and Eugster, 1965; Burkhard, 1991, 1993), (2) discriminate geotectonic settings (Nachit et al., 1985; Abdel-Rahman, 1994; Hecht, 1994; Shabani et al., 2003), (3) estimate crystallization temperature (Lühr et al., 1984), and (4) constrain the depth of crystallization (Uchida et al., 2007). Similarly, amphibole can also provide constraints on the crystallization conditions of granitic magma (c.f., Wones, 1981; Hammarstrom and Zen, 1986).

In this study, we present the chemistry of biotite and amphibole from the collision-related and post-collisional granites of the Guéra Massif with the aim to: (1) describe the mineral-chemical evolution of the mafic minerals from the granites of the Guéra Massif; (2) estimate magmatic conditions (pressure and temperature of crystallization, and oxygen fugacity) that prevailed during the crystallization of biotite; (3) characterize the geochemical differences in biotite between the collisional and the post-collisional granites, and (4) discuss the tectonomagmatic implications. The new data are used to constrain the secular evolution of magmatism as it changes from a collisional setting to a post-collisional setting. Moreover, the results provide additional constraints on the nature of crustal building processes within the Saharan Metacraton.

GEOLOGICAL BACKGROUND

The bedrock geology of Chad is characterized by the exposure of Late Ediacaran basement rocks within the Tibesti Massif in the north, Ouaddaï Massif in the east, Guéra Massif in the south-central part, and the Mayo Kebbi and Yadé massifs in the south (**Figure 1B**). The massifs are surrounded by younger sedimentary rocks, which include Lower Paleozoic sandstone sequences, Lower Cretaceous continental clastic rocks and Upper Cretaceous marine sediments in the north and northeast, Paleogene continental sediments in the south, and the Neogene lacustrine sediments (known as Chad Formation) of the Chad basin.

The Guéra Massif, also known as Massif Central tchadien (**Figure 2**), comprises magmatic and metamorphic rocks that developed during the Late Ediacaran collision between the Congo-São Francisco Craton and the Saharan Metacraton (Black, 1992; Kusnir and Schneider, 1995; Kusnir and Moutaye, 1997; Schlüter, 2008; Shellnutt et al., 2017, 2019b). Biotite granites are mainly exposed in the northern region near Mongo, which is intruded by gabbro whereas hornblende-biotite granites and hornblende granites and its fine grained equivalent are located in the east and south of the massif (**Figure 2**). A geochronological investigation of the granitic plutons shows that they are



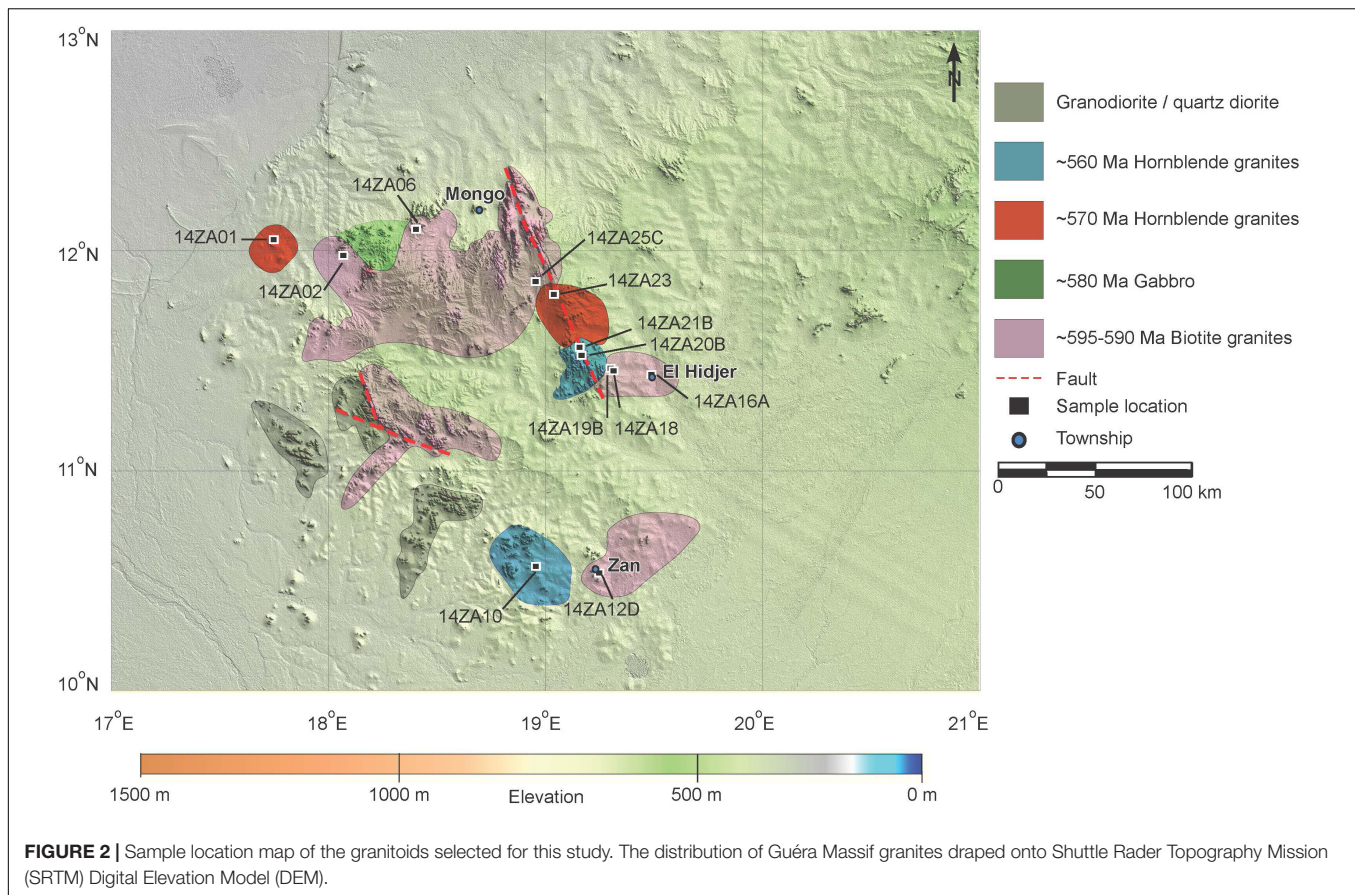
Neoproterozoic (595–560 Ma) in age and were subsequently buried under a sedimentary cover dominated by Quaternary alluvium (Kusnir and Schneider, 1995; Shellnutt et al., 2017; Pham, 2018). Cross-cutting the older (595–590 Ma) granites in the Mongo area are dolerite dykes that are oriented along/parallel to NNE–SSW, NE–SW, and ENE–WSW faults. They are described as vertical to sub-vertical dykes and extend over several kilometers. The Mongo doleritic dyke swarm intruded pre-existing fractures and may record the final stage of lithotectonic stabilization of the Guéra Massif (Nkouandou et al., 2017).

The ancient basement of the Guéra Massif is probably Meso- to Paleoproterozoic as inherited zircons of that age were identified within the collision-related granites (Shellnutt et al., 2017, 2019a). The collision-related granites are mostly biotite-granite, metaluminous to peraluminous, alkali calcic to calc-alkalic and magnesian to ferroan in composition, where the magnesian (~595 Ma) granites are similar to volcanic-arc granite and were emplaced before the ferroan (~590 Ma) syn-collisional granites (Supplementary Table S1; Frost et al., 2001; Pham, 2018; Shellnutt et al., 2019a). In contrast, the post-collisional

granites include biotite-granite and hornblende-biotite-granite, and are peraluminous to metaluminous, alkali calcic to calc-alkalic, and ferroan in composition. The compositionally similar ferroan rocks were emplaced at two distinct periods of ~570 and ~560 Ma (Supplementary Table S1; Pham, 2018). The whole rock compositions and zircon $^{206}\text{Pb}/^{238}\text{U}$ weighted-mean ages of the rocks in this study are summarized in Supplementary Table S1.

Sampling Locations of the Collision-Related Granites

Samples 14ZA02 (595 ± 8 Ma), 14ZA06, 14ZA25C are collected from three different locations of the same magnesian biotite-bearing granitic pluton surrounding Mongo (Figure 2). Each sample is about 50 km from each other. Sample 14ZA02 is located at the western part of the pluton (Figure 2). Sample 14ZA06 is located to the north whereas sample 14ZA25C is an amphibolite melanosome within gneissose granitoid located to the east (Figure 3A). The eastern outcrop was intruded by



younger granite that has not been dated. Sample 14ZA16A (593 ± 7 Ma) is a pink, ferroan granite that was intruded by a fine grained quartzofeldspathic dyke ~ 3 km east of El Hidjer (Figures 2, 3B). Sample 14ZA12D (589 ± 6 Ma) was collected from a granite outcrop about 20 km north of Zan. The textural, mineralogical, and age similarities of 14ZA16A and 14ZA12D suggests that they may be the same pluton.

Sampling Locations of the Post-collisional Granites

Sample 14ZA01 (568 ± 7 Ma) is a biotite-bearing gneissic granitoid collected ~ 100 km west of Mongo between Bakoro and Bitkin villages (Figure 2). This sample belongs to the westernmost pluton of the study and is texturally and mineralogically different from the older Mongo granite (Figures 2, 4A). Sample 14ZA23 (568 ± 6 Ma) was collected ~ 50 km to the southeast of Mongo, halfway between Mongo and El Hidjer (Figure 2).

Samples 14ZA20B and –21B were collected about 50 km west of El Hidjer (Figure 2). The outcrop exposes multiple magmatic rocks ranging from biotite-hornblende gneissose enclave to NW-SE striking steep dipping foliated gneissic granite (14ZA20B) truncated by younger mafic intrusions, and quartzofeldspathic veins (Figures 4B,C). Sample 14ZA21B is coarse grained granite that contains darker microgranular enclaves. Pink granite

samples 14ZA18 and ZA1419B (561 ± 6 Ma) were collected from a pluton with an exfoliation dome-like structure ~ 30 km west of El Hidjer that is texturally different from the pluton in which samples 14ZA20B and 14ZA21B were collected (Figure 2). The granite is composed of coarse grained K-feldspar, plagioclase, biotite, hornblende with concentrated patches of amphibolite xenoliths. Sample 14ZA10 (556 ± 7 Ma) is biotite-bearing granite with centimeter size feldspar phenocrysts collected from one of the southernmost plutons ~ 30 km west of Zan. The granites are slightly deformed as there is an alignment of biotite (Figure 4D).

The Lake Fitri inliers are located to the northwest of the Guéra Massif and comprise fresh and coarse-grained biotite-bearing granites (Figures 1C,D). They are exposed as lenticular to ellipsoidal granitic hills up to several kilometers in length and less than 1 km wide near or between the communities of Ngoura and Moyto. Generally, the Lake Fitri granites have similar texture, mineralogy (biotite, quartz, K-feldspar), whole-rock chemistry (peraluminous to metaluminous, alkali calcic to calc-alkalic, high potassium and ferroan) and Nd isotopic compositions (Shellnutt et al., 2018). Moreover, they are somewhat compositionally similar to the post-collisional granites of the Guéra Massif but are slightly younger (554 ± 8 and 546 ± 8 Ma) and have moderately depleted Nd isotopic compositions [$\epsilon_{Nd}(t) = +1.3$ to $+2.9$] as opposed to the enriched Nd isotopes [$\epsilon_{Nd}(t) = -13.1$ to $+0.2$] of the rocks from the Guéra Massif (Pham, 2018; Shellnutt et al., 2018). Biotite compositions from the granitic rocks at Ngoura

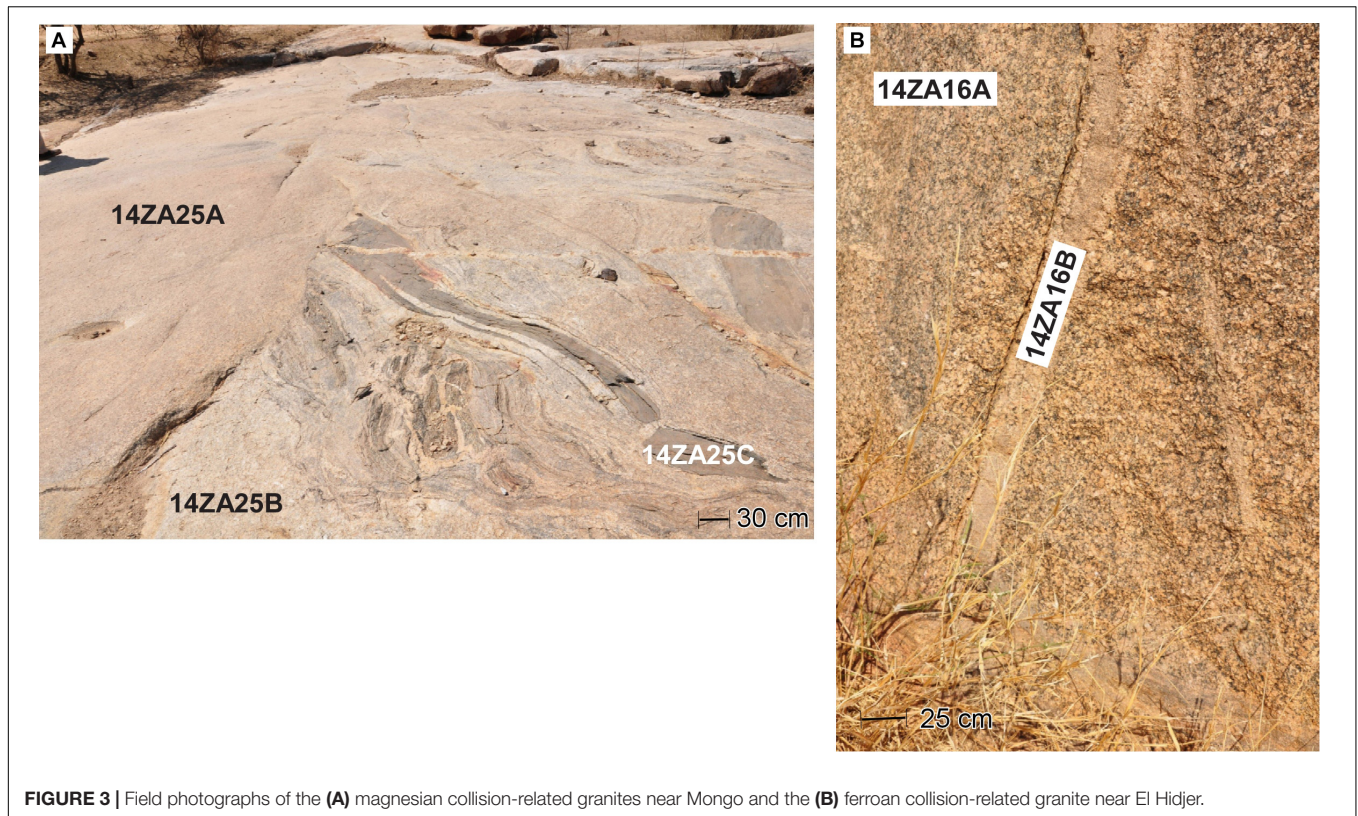


FIGURE 3 | Field photographs of the (A) magnesian collision-related granites near Mongo and the (B) ferroan collision-related granite near El Hidjer.

and Moyto were presented by Shellnutt et al. (2018) and are discussed in this paper.

PETROGRAPHY

Collision-Related Granitic Rocks

The collisional granites include both hornblende-biotite granite (590 Ma group) and biotite granite (595 Ma group) that vary from coarse-grained and granular to fine grained. Exsolution textures, such as perthite and myrmekite, are common in both groups. The 590 Ma collisional granites (Figures 5A,B) are primarily composed of plagioclase (10–20 vol.%), K-feldspar (35–45 vol.%), biotite (8–10 vol.%), and quartz (20–30 vol.%) with accessory amounts of amphibole (1–2 vol.%), opaques (Fe-Ti oxide and sulfide minerals), zircon, and apatite. The plagioclase crystals display albite twinning. The K-feldspar crystals are medium- to coarse grained (0.5–1 mm or larger), and commonly have subsolidus exsolution (cross-hatched twinning perthite) and lamellar exsolution. Some of the K-feldspar is altered to clay minerals and secondary muscovite. The biotite crystals are coarse-grained and ≤ 2 mm in length, have greenish brown to brown pleochroism, and contain inclusions of apatite and zircon (metamict halo). The quartz crystals are fine- to coarse-grained (0.75–1 cm), fractured, and have undulose extinction. In comparison, the 595 Ma granites (Figures 5C,D) have the same mineral assemblage of plagioclase (10–20 vol.%), K-feldspar (25–50 vol.%), biotite (15–17 vol.%), and quartz (20–30 vol.%)

with opaque accessory (Fe-Ti oxide and sulfide minerals), zircon, secondary muscovite, and apatite but amphibole was not observed. The rocks have similar mineral textures as ~ 590 Ma rocks but the biotite crystals were generally more abundant and have green to greenish brown pleochroism.

Post-collisional Granitic Rocks

The post-collisional granites are mostly hornblende-biotite granites and are coarse-grained and granular (Figure 6). The most distinguishing feature between younger (~ 560 Ma) and older (~ 570 Ma) post-collisional granites is the abundance of amphibole (hornblende) that can be up to 15–20 vol.% (sample 14ZA20B). These rocks are generally fresh, but some crystals of quartz and K-feldspar are cloudy. Exsolution textures such as perthite and myrmekite are common (Figure 6A). The 560 Ma group has a mineral assemblage of amphibole (~ 2 –20 vol.%), plagioclase (8–10 vol.%), biotite (2–10 vol.%), K-feldspar (30–50 vol.%), quartz (20–40 vol.%), and accessory (1–3 vol.%) minerals (Figures 6B–D). Most of the amphibole crystals are hornblende that are identified by deep-green to light-green pleochroism. In some cases the hornblende is altered to a mixture of reddish-brown oxyhornblende and oxide (hematite, rutile) minerals (Figure 6D). The plagioclase phenocrysts (0.5–2.25 mm) have albite and polysynthetic twinning. The biotite crystals are observed as both phenocrysts and inclusions within K-feldspar but the phenocrysts are commonly interstitial to other minerals and have pale yellow-brown to pale brown pleochroism. The K-feldspar crystals are medium to coarse-grained and regularly

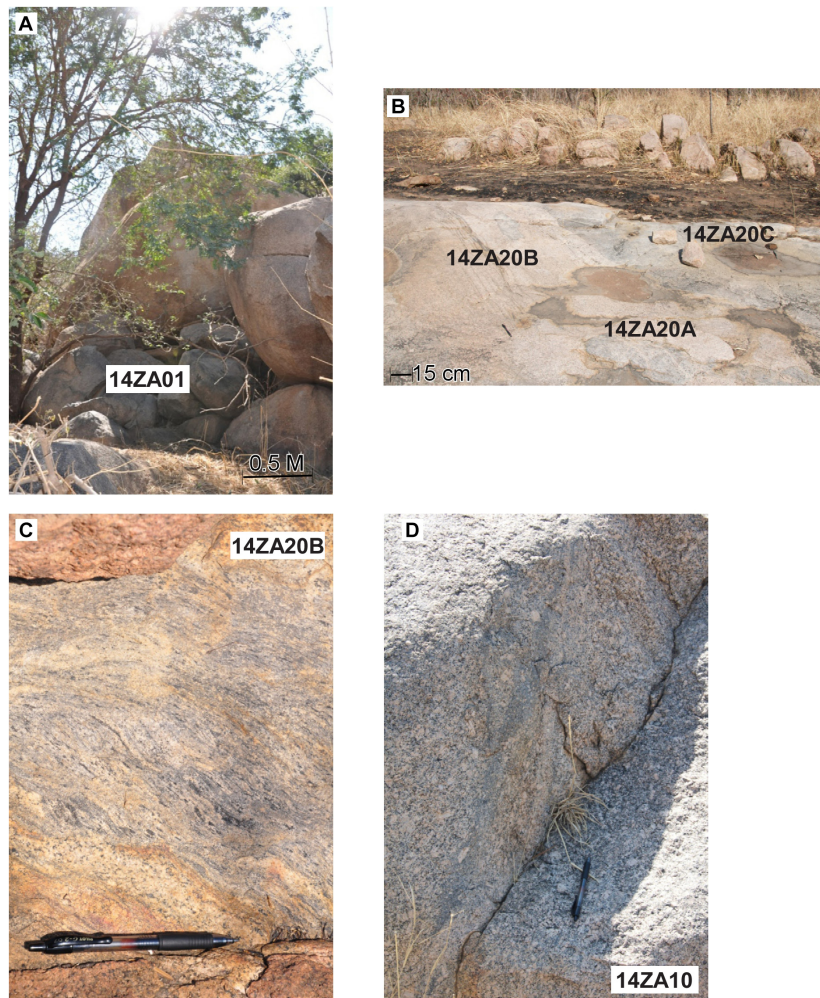


FIGURE 4 | (A) Field photograph of the ~570 Ma post-collisional granites west of Mongo. Field photographs of ~560 Ma post-collisional granites west of El Hidjer **(B,C)** and near Zan **(D)**.

exhibit Carlsbad or microcline twinning. There are some alkali feldspar crystals with perthite exsolution lamellae. The quartz crystals are fractured, randomly oriented, and have variable grain sizes. Accessory minerals include: zircon, muscovite, chlorite and opaques. The 570 Ma granites have a similar mineral assemblage of plagioclase (15–20 vol.%), K-feldspar (35–40 vol.%), biotite (8–10 vol.%), quartz (20–25%) with similar accessory minerals (<3 vol.% of chlorite, zircon and opaques), but tend to have less amphibole (3–4 vol.%) as compared to the 560 Ma granites (**Figures 6E,F**).

MATERIALS AND METHODS

To investigate the mineralogical composition of the Guëira Massif granites a total of twelve samples of biotite-granite and hornblende-biotite-granite were selected for analysis by electron probe micro-analyzer (EPMA). The EPMA used for this study is a JEOL JXA-8500F, equipped with five WDS

at EPMA laboratory in the Institute of Earth Sciences, Academia Sinica, Taipei. The equipment operated at 16 kV voltage and 6 nA current beam with a 2 mm diameter electron beam. The ZAF method using the standard calibration of synthetic chemical-known standard minerals with diverse diffracting crystals used to correct the X-ray intensities, are as follows: wollastonite for Si with TAP crystal, rutile for Ti (PET), corundum for Al (TAP), Cr-oxide for Cr (PET), hematite for Fe (LiF), Mn-oxide for Mn (PET), periclase for Mg (TAP), Ni-oxide for Ni (LiF), Co-oxide for Co (LiF), wollastonite for Ca (PET), albite for Na (TAP), orthoclase for K (PET), Zn-oxide for Zn (LiF), apatite for P (PET), fluorite for F (TAP), tugtupite for Cl (PET) and anhydrite for S (PET). The relative standard deviations (RSD) for F, Cl, S, and P were less than 2%, for Si, Na, and K were less than 1%, and other elements were less than 0.5%. The detection limits for F, Cl, S, and P were less than 0.5 wt%. The analysis results are shown in **Supplementary Table S1**.

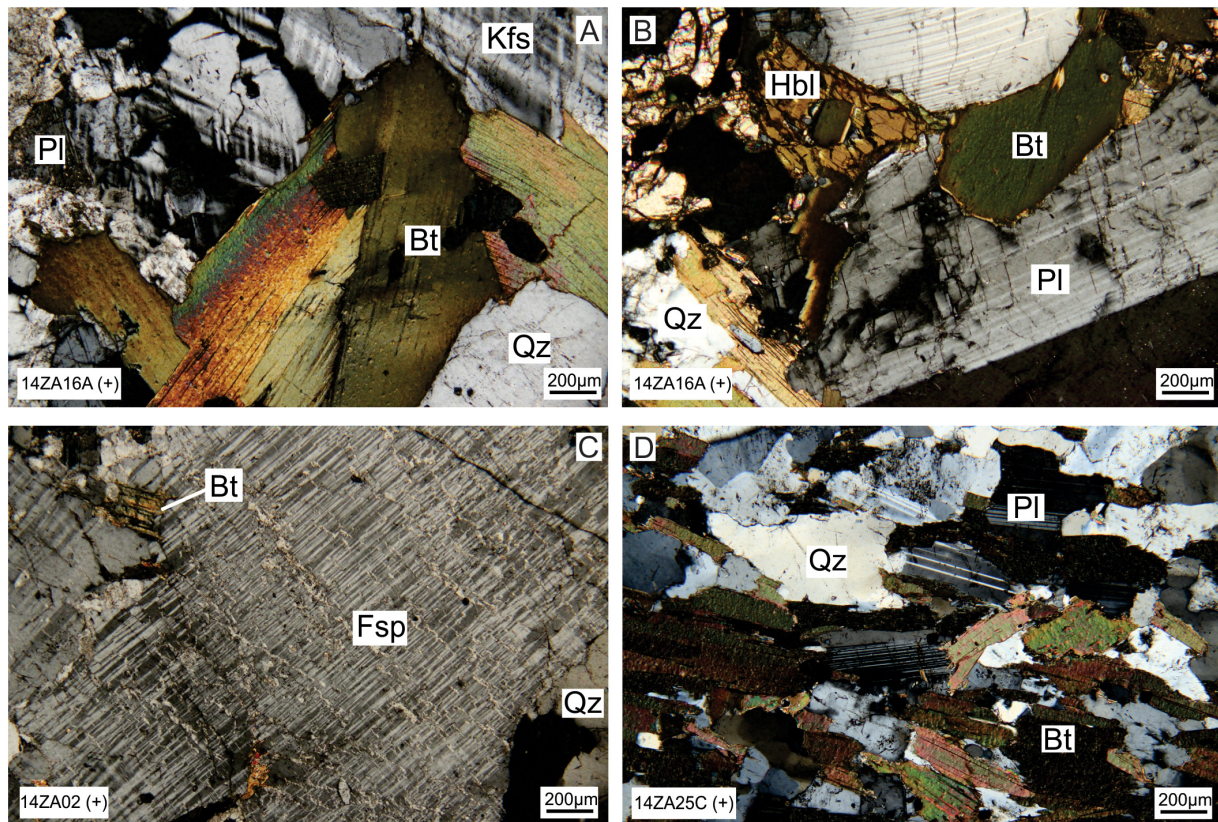


FIGURE 5 | Photomicrographs of the Guéra Massif collisional granites under crossed polarizers. Panels (A,B) are from 14ZA16A of the 590 Ma granites, and (C) 14ZA02, and (D) 14ZA25C of the 595 Ma granites. Qz, quartz; Pl, plagioclase; Bt, biotite; Kfs, potassium feldspar; Fsp, perthitic feldspar; Hbl, hornblende.

The structural formulae of biotite were calculated on the basis of 22 oxygen equivalents without H_2O^+ and 13 cations by using the Excel spreadsheet program designed by Tindle and Webb (1990). For this study, only the biotite results that classify as “primary magmatic biotite” are considered (Nachit et al., 2005). The partitioning of Fe^{3+} and Fe^{2+} from the total iron (FeO^t) was calculated by charge balance using the program “Fe23” (Nenova, 1997). It is reported that the calculated Fe^{2+} and Fe^{3+} deviate from the experimental derived contents by less than 1%. The chemical formulae of amphibole are recalculated on the basis of 23 oxygens equivalents with $\text{Fe}^{2+}/\text{Fe}^{3+}$ estimation, without H_2O^+ , and 13 cations using the program Probe-AMPH (Tindle and Webb, 1994). The chemical formula, geochemical features of amphibole and biotite, and their computed stoichiometry are summarized and listed in **Supplementary Table S1**. Biotite chemistry from the Lake Fitri granites, reported by Shellnutt et al. (2018), will also be discussed in relation to the Guéra Massif granites.

RESULTS

Collisional-Related Granites

There are distinct compositional differences between the biotite crystals from the 590 Ma (14ZA12D, -16A) and 595 Ma

(14ZA02, -06, -25C) collision-related intrusions. The 590 Ma granites samples tend to have similar Al_2O_3 (13.23–16.21 wt.%) and TiO_2 (1.32–3.84 wt.%) but lower MgO (0.64–6.66 wt.%), and higher FeO^t (26.43–34.46 wt.%), and Fe# (0.70–0.98) than the biotite crystals of 595 Ma granites ($\text{Al}_2\text{O}_3 = 13.94$ –17.53 wt.%; $\text{TiO}_2 = 1.12$ –4.05 wt.%; MgO = 7.48–13.68 wt.%; $\text{FeO}^t = 13.07$ –23.33 wt.%; Fe# = 0.46–0.62). Furthermore, the biotite from the 590 Ma rocks classify as siderophyllite whereas the biotite from the 595 Ma rocks classify as Fe-biotite (Foster, 1960).

The calcic amphibole (ferro-edenite to ferro-pargasite) crystals from the 590 Ma collision-related granites (14ZA12D, -16A) are fairly homogeneous within each sample but between samples there is significant variability of the major elements. The amphibole from sample 14ZA12D has higher SiO_2 (>41 wt%) and MnO (>0.7 wt%) but lower TiO_2 (<1 wt%), Al_2O_3 (<8.7 wt%), Na_2O (<1.7 wt%), and K_2O (≤ 1 wt%) compared to 14ZA16A ($\text{SiO}_2 < 40$ wt%; $\text{TiO}_2 > 0.8$ wt%, $\text{Al}_2\text{O}_3 > 10.4$ wt%; MnO < 0.7 wt%; $\text{Na}_2\text{O} > 1.3$ wt%; $\text{K}_2\text{O} > 1.6$ wt%).

Post-collisional Granites

The compositions of the biotite crystals from the 560 Ma granites (14ZA01, -10, -18, -19B, -20B, -21B, 23) are similar ($\text{Al}_2\text{O}_3 = 12.35$ –17.17 wt.%; $\text{TiO}_2 = 2.48$ –4.02 wt.%; MgO = 0.30–5.13 wt.%; $\text{FeO}^t = 26.50$ –35.35 wt.%) to the biotite crystals from

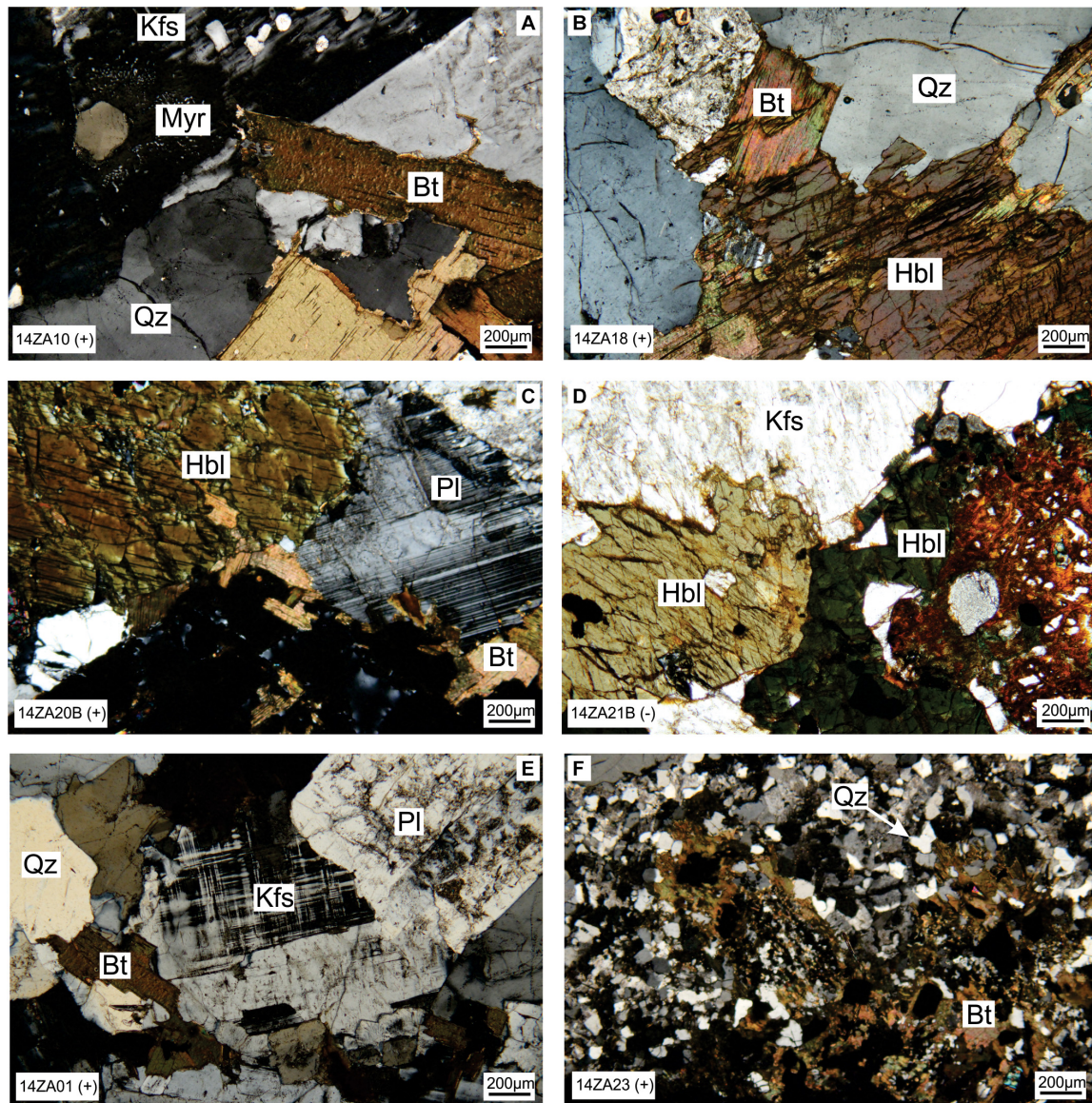


FIGURE 6 | Photomicrographs of the Guéra Massif post-collisional granites under crossed polarizers. (A) 14ZA10, (B) 14ZA18, (C) 14ZA20B, and (D) 14ZA21B of the 560 Ma granites. (E) 14ZA01, and (F) 14ZA23 of the 570 Ma granites. Qz, quartz; Pl, plagioclase; Bt, biotite; Kfs, potassium feldspar; Myr, myrmekite; Hbl, hornblende.

570 Ma (14ZA01, -23) granites ($\text{Al}_2\text{O}_3 = 10.94\text{--}15.26$ wt%; $\text{TiO}_2 = 2.35\text{--}4.88$ wt%; $\text{MgO} = 0.68\text{--}5.46$ wt%; $\text{FeO}^t = 24.70\text{--}35.35$ wt%). All biotite are Fe-rich (siderophyllite) and have similar Fe# values (0.73–0.98).

The amphibole crystals from the post-collisional (560 Ma = 14ZA18, -19B, -20B, 21B; 570 Ma = 14ZA01, -23) intrusions are calcic (ferro-edenite to ferro-pargasite). The compositions of the amphibole from the 560 Ma rocks are generally similar to each other ($\text{SiO}_2 = 45.2\text{--}36.2$ wt%, $\text{TiO}_2 = 2.3\text{--}0.3$ wt%, $\text{Al}_2\text{O}_3 = 9.6\text{--}5.0$ wt%, $\text{MnO} = 0.9\text{--}0.2$ wt%, $\text{CaO} = 11.0\text{--}8.4$ wt%, $\text{Na}_2\text{O} = 2.0\text{--}0.5$ wt%, $\text{K}_2\text{O} = 2.9\text{--}0.7$ wt%, $\text{Fe}\# = 0.80\text{--}0.74$) but slightly different from those analyzed from the 570 Ma rocks ($\text{SiO}_2 = 41.2\text{--}40.6$ wt%, $\text{TiO}_2 = 2.0\text{--}0.9$

wt%, $\text{Al}_2\text{O}_3 = 9.1\text{--}8.2$ wt%, $\text{MnO} = 0.9\text{--}0.6$ wt%, $\text{CaO} = 10.9\text{--}10.3$ wt%, $\text{Na}_2\text{O} = 2.2\text{--}1.5$ wt%, $\text{K}_2\text{O} = 1.3\text{--}1.1$ wt%, $\text{Fe}\# = 0.81\text{--}0.78$). Only two analysis were obtained from sample 14ZA23.

DISCUSSION

Biotite Crystallization Temperature Estimates

The presence of ilmenite and magnetite in granitic rocks is a common mineral pairing used to estimate magmatic temperature of silicic igneous rocks (Buddington and Lindsley, 1964; Ghiorso and Sack, 1991; Anderson et al., 1993). However, the temperature

sensitivity of Ti and Ti/Fe^{2+} in biotite can also be used to obtain reliable temperature estimations in igneous and metamorphic rocks (Lühr et al., 1984). The granitic rocks from the Guéra Massif are primarily composed of plagioclase, K-feldspar, and quartz but have significant amounts (5–15 vol.%) of hornblende and biotite with accessory (<5 vol.%) amounts of apatite, Fe-Ti oxide minerals (ilmenite, magnetite), and sulfide minerals are also present. Consequently, we are able to use the equation of Lühr et al. (1984) to calculate the biotite crystallization temperatures based on the coupled exchange of Ti and Fe^{2+} in biotite. The temperatures are calculated from Eq. (1).

$$T(K) = \frac{838}{1.0337 - \frac{\text{Ti}}{\text{Fe}^{2+}}} \quad (1)$$

The maximum, minimum, and average crystallization temperatures of the biotite from the Guéra Massif and Lake Fitri inliers are listed in **Table 1** with the entire data set presented in **Supplementary Table S1**. Overall, the biotites from the collisional granites tend to have higher average crystallization temperatures than the post-collisional granites from Guéra Massif and the Lake Fitri region (**Figures 7A,B**). Specifically, the results from sample 14ZA02 (595 Ma) have the highest temperature (723°C) and average temperature ($696 \pm 37^\circ\text{C}$). The other two remaining 595 Ma rocks have the second (14ZA25 = $666 \pm 42^\circ\text{C}$) and the fifth highest average temperatures (14ZA06 = $633 \pm 21^\circ\text{C}$). In comparison, the 590 Ma rocks have lower average temperatures (14ZA16A = $619 \pm 22^\circ\text{C}$; 14ZA12D = $612 \pm 8^\circ\text{C}$). The post-collisional granites have lower average temperatures overall but overlap with 590 Ma collisional rocks (630 ± 26 – $607 \pm 7^\circ\text{C}$). The Lake Fitri post-collisional rocks are somewhat different from the Guéra Massif rocks. The

biotite from the Ngoura rocks yields higher average temperatures (634 ± 21 , 639 ± 18 , $625 \pm 20^\circ\text{C}$) than the biotite from the younger Moyto granites ($612 \pm 13^\circ\text{C}$).

Amphibole Pressure Estimates

Emplacement pressure estimates of granitic rocks can be calculated based on the Al content of hornblende providing the host rocks contain the requisite mineral assemblages (Hammarstrom and Zen, 1986; Hollister et al., 1987; Johnson and Rutherford, 1989; Schmidt, 1992). There are concerns regarding the constraints for an accurate geobarometer estimate using amphibole given all of the parameters that could potentially affect the results (Hollister et al., 1987; Ghent et al., 1991). Although, the computed pressure may display the depth at which the hornblende crystallizes, it may not indicate the pressure at which the granite reached neutral buoyancy (i.e., emplacement depth) in the crust because it is likely that the majority of minerals crystallize after hornblende (Ghent et al., 1991).

We find that the hornblende geobarometers of Hammarstrom and Zen (1986) and Johnson and Rutherford (1989) are better suited for our samples as the mineral assemblages are ideal and our results are closest to their calibration curves. However, we prefer the geobarometer of Johnson and Rutherford (1989) due to better constraints on the pressure uncertainty (i.e., ± 0.5 kbar). The amphibole crystallization pressure of the Guéra Massif granitic rocks is calculated using Eq. (2).

$$P(\pm 0.5 \text{ kbar}) = 3 - 3.46 (\pm 0.24) + 4.23 (\pm 0.13) (\text{Al}^{\text{I}})^T \quad (2)$$

Where Al^{I} designates the total number of Al atoms in amphibole based on 23 oxygen equivalents. The calibration is based on the relation between Al^{I} in hornblende and pressure for calc-alkalic granitic rocks that are made of up of an igneous mineral assemblage consisting of hornblende, plagioclase, biotite, K-feldspar, quartz, titanite, and magnetite or ilmenite. The results indicate that the crystallization of hornblende occurred between ~ 0.1 and 0.6 GPa across all samples but the ~ 590 Ma collisional rocks have the greatest variability (**Table 2** and **Supplementary Table S1**; **Figure 7C**). Amphibole is not present in all of the studied samples. Thus, there is a limited application of this method across all granitic rocks from the Guéra Massif granites.

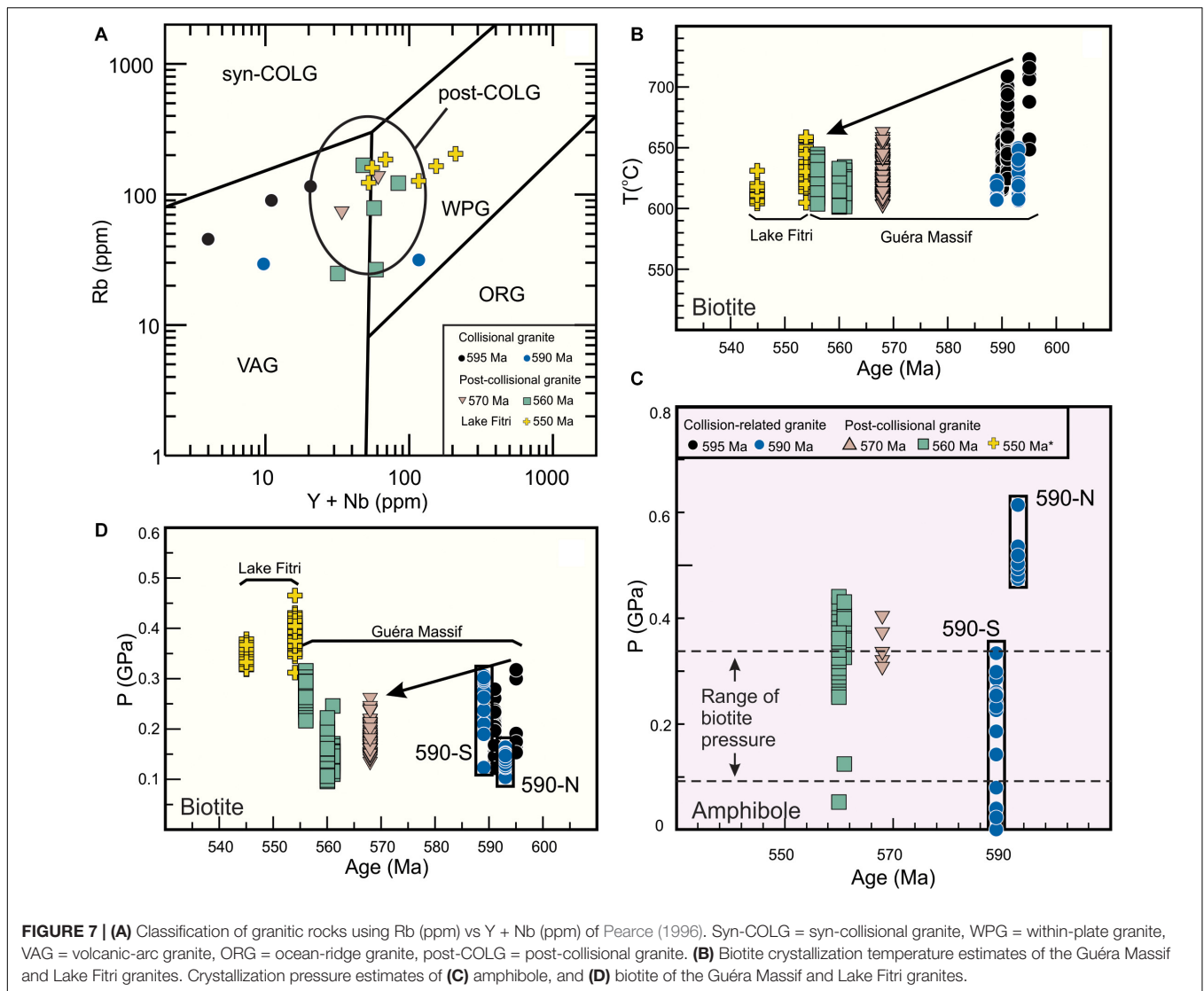
Biotite Pressure Estimates

The concentration of TiO_2 and Al^{VI} in biotite is linked to the emplacement depth of its host pluton. In particular, granites with biotite that have low TiO_2 and high Al^{VI} content are typical for an abyssal depth of formation. Furthermore, granites that crystallize at deeper depth are characterized by high TiO_2 and Al^{VI} content (Machev et al., 2004; Bora and Kumar, 2015). In this study, the TiO_2 and Al^{VI} contents in biotite of collisional granite are $\text{TiO}_2 = 2.19$ – 4.05 wt%, $\text{Al}^{\text{VI}} = 0.05$ – 0.9 apfu. The values of the post-collisional granites are as follows: $\text{TiO}_2 = 2.35$ – 4.88 wt%, $\text{Al}^{\text{VI}} = 0.07$ – 0.48 apfu, for 570 Ma granite; $\text{TiO}_2 = 2.48$ – 4.02 wt%, $\text{Al}^{\text{VI}} = 0.10$ – 0.74 apfu, for 560 Ma granite; $\text{TiO}_2 = 1.3$ – 4.0 wt%, $\text{Al}^{\text{VI}} = 0.46$ – 1.15 apfu, for Lake Fitri granite. The Lake Fitri post-collisional granites have relatively high Al^{VI} contents and low TiO_2 content, potentially indicating the highest pressure

TABLE 1 | The range of crystallization temperature estimates of biotite from the granites of the Guéra Massif and Lake Fitri region.

Pluton	Sample	Temperature ($^\circ\text{C}$)		
		Max	Min	Average
595 Ma	14ZA02	723	648	696 ± 37
595 Ma	14ZA06	658	615	633 ± 21
595 Ma	14ZA25C	708	624	666 ± 42
590 Ma-N	14ZA16A	650	606	619 ± 22
590 Ma-S	14ZA12D	623	606	612 ± 8
570 Ma-W	14ZA01	659	606	630 ± 26
570 Ma-E	14ZA23	663	603	619 ± 30
560 Ma-S	14ZA10	644	604	626 ± 20
560 Ma-N	14ZA18	614	601	607 ± 7
560 Ma-N	14ZA19B	634	601	619 ± 16
560 Ma-N	14ZA20B	628	602	614 ± 13
560 Ma-N	14ZA21B	633	602	614 ± 15
550 Ma Ngoura	NA01	656	614	634 ± 21
550 Ma Ngoura	NA03	659	624	639 ± 18
550 Ma Ngoura	NA06	645	605	625 ± 20
550 Ma Moyto 2	NA18	631	604	612 ± 13

Average = average value of the temperature in Celsius including the uncertainty in the average.



of crystallization among the studied granites. The relatively high TiO_2 and Al^{VI} contents in the Guéra Massif granites are supportive of a mid-crustal level crystallization depth.

Uchida et al. (2007) demonstrated that the total Al content of amphibole and total Al content of biotite increase together with increasing pressure, in other words, the crystallization pressure of granitoids may be constrained by the total concentration of Al in biotite. Therefore, Al-in-biotite can be utilized instead of the Al-in-hornblende for geobarometry estimates where appropriate. Eq. (3) is used to calculate crystallization pressure of biotite in granitic rocks that contain a mineral assemblage of plagioclase + biotite + muscovite + hornblende + K-feldspar + magnetite + ilmenite.

$$P \text{ (kbar)} = 3.33\text{Al}^{\text{t}} - 6.53 (\pm 0.33) \quad (3)$$

Where Al^{t} designates the total number of Al atoms in biotite on the bases of 22 oxygen equivalents.

The calculated average biotite crystallization pressures are shown in **Figure 7D**. The average values for individual plutons are summarized in **Table 3** with the complete results in **Supplementary Table S1**. The data indicate that the biotite crystallization pressure of the collisional granites tends to be more restricted (0.19 ± 0.08 – 0.23 ± 0.03 GPa) for the older granites than that for the younger granites (0.13 ± 0.02 – 0.25 ± 0.09 GPa) although they overlap. The biotite from the post-collisional granites, including those from Lake Fitri, have variable average pressures (570 Ma = 0.17 ± 0.05 and 0.17 ± 0.07 GPa; 560 Ma = 0.14 ± 0.07 – 0.27 ± 0.05 GPa; Lake Fitri = 0.35 ± 0.03 – 0.39 ± 0.08 GPa) but, the Lake Fitri rocks have the highest estimates.

Oxygen Fugacity Estimates

Oxygen fugacity (f_{O_2}) is an essential parameter constraining magmatic activities (Kilinc et al., 1983; Kress and Carmichael, 1991; Ottonello et al., 2001; Botcharnikov et al., 2005). It

TABLE 2 | The range of amphibole pressure estimates from the Gueira Massif granites.

Pluton	Sample	Pressure (GPa)		
		Max	Min	Average
590 Ma-N	14ZA16A	0.61	0.47	0.50 ± 0.07
590 Ma-S	14ZA12D	0.33	0.02	0.20 ± 0.15
570 Ma-W	14ZA01	0.37	0.31	0.33 ± 0.03
570 Ma-E	14ZA23	0.40		
560 Ma-N	14ZA18	0.44	0.32	0.39 ± 0.06
560 Ma-N	14ZA19B	0.43	0.12	0.37 ± 0.15
560 Ma-N	14ZA20B	0.36	0.05	0.29 ± 0.15
560 Ma-N	14ZA21B	0.37	0.25	0.33 ± 0.06

GPa = gigapascal. The uncertainty for all calculations is ±0.05 GPa (Johnson and Rutherford, 1989). Sample 14ZA23 only has one analysis. Average = average value of the pressure (GPa) including the uncertainty in the average.

is considered to be a useful tool for determining the redox condition of melts during petrogenesis, due to its effect on crystallization, differentiation, and geophysical properties (e.g., melt structure and viscosity) of magma (Carmichael, 1991; Jayasuriya et al., 2004).

Equation (4) is used to calculate the oxygen fugacity estimate of Eugster and Wones (1962). It is based upon the Fe²⁺-Fe³⁺-Mg²⁺ composition of biotite, and the P and T for various oxygen buffers.

$$\text{Log}fO_2 = -\frac{A}{T} + B + C\frac{(P-1)}{T} \quad (4)$$

Where *T* is the temperature in K, *P* is the pressure in bar, and A, B, and C are corresponding coefficients for different oxygen fugacity buffers. Temperature is calculated using equation (1), and P is calculated using equation (3).

The calculation of *f*O₂ depends on the value of coefficients A, B, and C that represent different oxygen fugacity buffers (Eugster and Wones, 1962). The coefficients are chosen based on the proportions of Fe²⁺, Fe³⁺, and Mg²⁺ in biotite, which for this study, are calculated using the methods of Nenova (1997). Wones and Eugster (1965) established the Fe²⁺-Fe³⁺-Mg²⁺ ternary diagram using the contents of biotite, where the QFM (quartz-fayalite-magnetite), NNO (Ni-NiO), and HM (hematite-magnetite) buffers are defined based on experimental data. In ideal cases, the A, B, and C values are able to be directly obtained from Eugster and Wones (1962) for a given buffer, if the data plot directly on one of the buffers. In fact, there are many cases of biotite straddling two buffers in this study. The corresponding value of the coefficient was assigned to the buffer that is closest to the data point (Yavuz, 2003a,b; Ayati et al., 2013; Li et al., 2017). In this study, all samples plot along with the QFM and NNO buffers (Figure 8), therefore, the value of A, B, and C coefficients are interpolated between these buffers. In which, the QFM buffer is used for Moyto (Lake Fitri), 560 Ma-N (northern) pluton, 570 Ma-E (eastern pluton), and the 590 Ma pluton whereas the NNO buffer is designated for Ngoura (Lake Fitri), 560 Ma-S (southern) pluton, 570 Ma-W (western) pluton, and 595 pluton (Table 4). The average values of log *f*O₂ and their corresponding

TABLE 3 | The range of biotite pressure estimates of the Gueira Massif and Lake Fitri granites.

Pluton	Sample	Biotite Pressure (GPa)		
		Max	Min	Average
595 Ma	14ZA02	0.317	0.153	0.21 ± 0.08
595 Ma	14ZA06	0.261	0.208	0.23 ± 0.03
595 Ma	14ZA25C	0.279	0.122	0.18 ± 0.08
590 Ma-N	14ZA16A	0.164	0.104	0.13 ± 0.02
590 Ma-S	14ZA12D	0.305	0.123	0.25 ± 0.09
570 Ma-W	14ZA01	0.225	0.121	0.17 ± 0.05
570 Ma-E	14ZA23	0.262	0.136	0.18 ± 0.06
560 Ma-S	14ZA10	0.315	0.216	0.27 ± 0.05
560 Ma-N	14ZA18	0.166	0.096	0.14 ± 0.03
560 Ma-N	14ZA19B	0.245	0.110	0.14 ± 0.07
560 Ma-N	14ZA20B	0.202	0.095	0.14 ± 0.06
560 Ma-N	14ZA21B	0.222	0.160	0.19 ± 0.03
550 Ma Ngoura	NA01	0.430	0.344	0.39 ± 0.05
550 Ma Ngoura	NA03	0.427	0.349	0.39 ± 0.04
550 Ma Ngoura	NA06	0.465	0.312	0.39 ± 0.08
550 Ma Moyto 2	NA18	0.378	0.318	0.35 ± 0.03

GPa = gigapascal. The uncertainty of each calculation is ±0.033 GPa (Uchida et al., 2007). Average = average value of the pressure (GPa) including the uncertainty in the average.

values to ΔQFM are summarized in Table 4 and the results are listed in Supplementary Tables S2, S3.

The estimates do not indicate a secular variation but it seems that the granites around Mongo are generally more oxidizing (ΔQFM +0.3 to +0.5) whereas the granites to the east and south are generally more reducing (ΔQFM − 1). The granites from Lake Fitri shows a similar range of estimates with the Ngoura rocks (ΔQFM + 0.3) being moderately oxidizing and the Moyto rocks (ΔQFM − 1) being reducing.

Secular Variation in the Guéra Massif Granites

The estimated temperatures and to some extent pressures of the biotite from the Guéra Massif granites show a systematic variation from higher to lower values with decreasing age. The biotite crystallization temperatures from the Guéra Massif and the Lake Fitri region show a secular variation as they drop from 696 ± 37–607 ± 7°C over time (Figure 7B). The low temperatures of some biotite (<650°C) is indicative of late stage crystallization. Experimental studies show that granitic magma will become solid when the solidification temperature cools to 650–700°C (Tuttle and Bowen, 1958; Luth et al., 1964; Piwinski, 1968; Freiberg et al., 2001). However, recent studies suggest that the crystallization of many minerals, in particular K-feldspar megacrysts, in calc-alkalic granites can be lower than 650°C and argue for lower consolidation temperatures due to repeated cycles of heating and fluxing by water-rich fluids (Glazner and Johnson, 2013; Challener and Glazner, 2017).

In comparison, the zircon saturation temperature estimates (TZr°C ± 40°C) do not show a secular variation as the temperatures for all rocks ranges from 714°C to 587°C

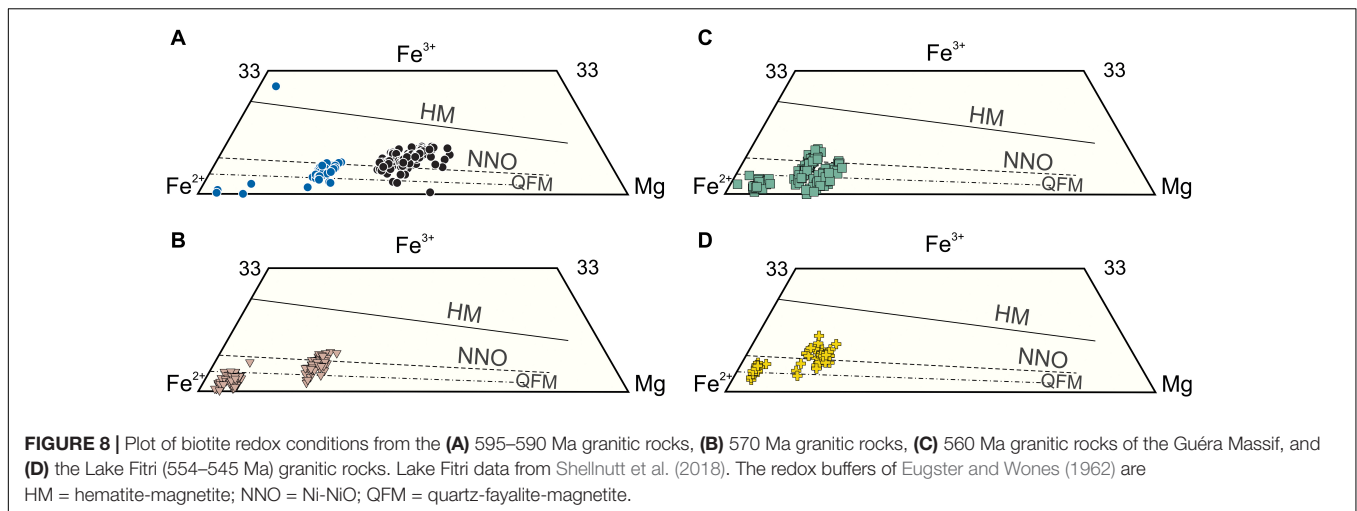


TABLE 4 | The range of biotite oxygen fugacity estimates from the Gueira Massif and Lake Fitri granites.

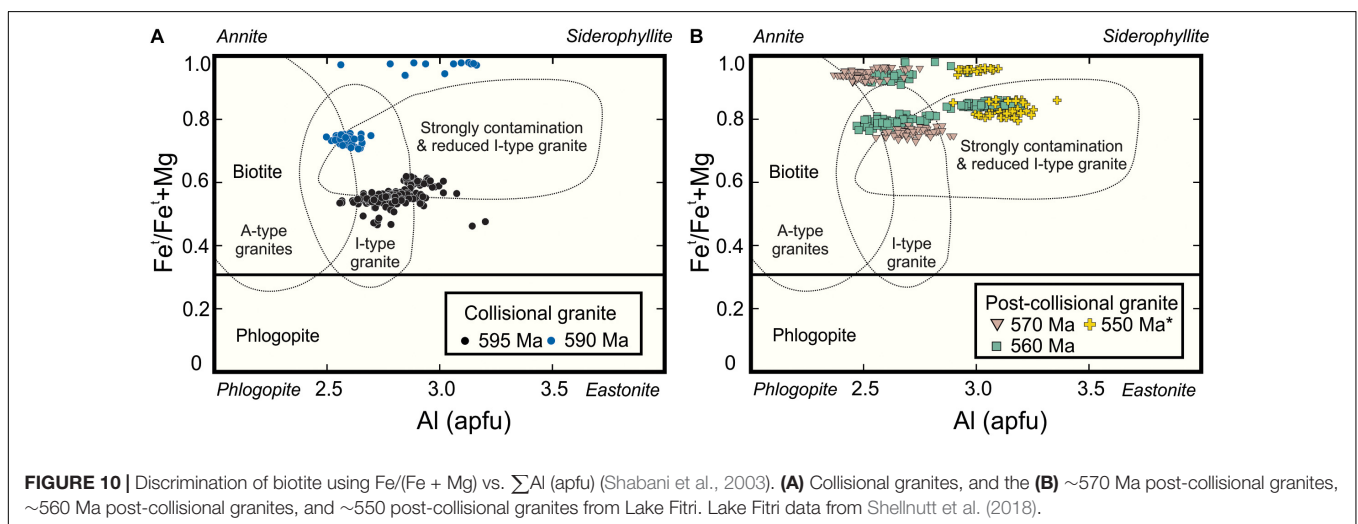
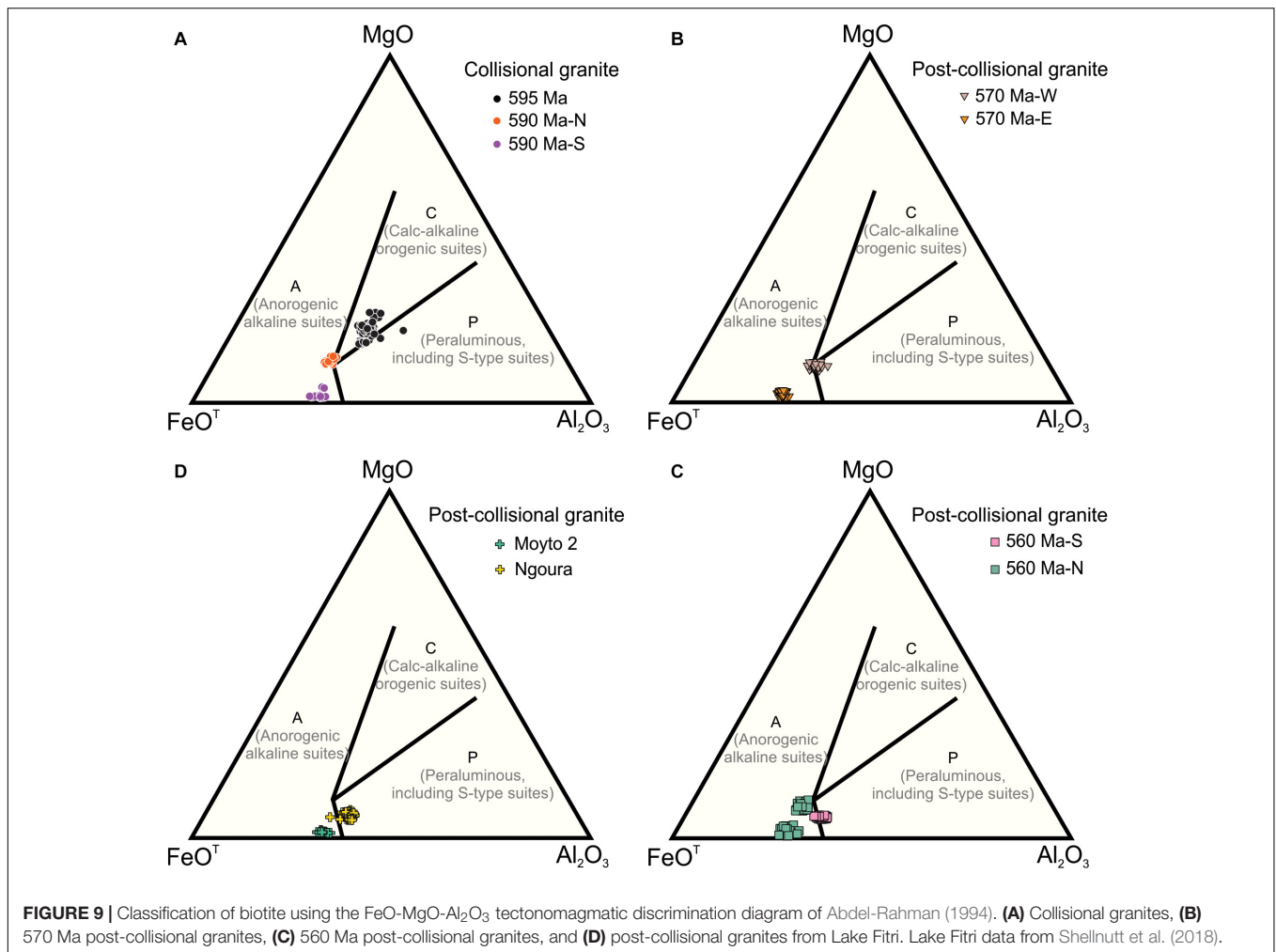
Pluton	Sample	LogfO ₂			ΔQFM (Average)	Buffer
		Max	Min	Average		
595 Ma	14ZA02	-15.80	-17.73	-16.5 ± 1.0	+0.30 ± 0.03	NNO
595 Ma	14ZA06	-17.50	-18.77	-18.2 ± 0.6	+0.41 ± 0.05	NNO
595 Ma	14ZA25C	-16.17	-18.51	-17.3 ± 1.2	+0.37 ± 0.09	NNO
590 Ma-N	14ZA16A	-19.17	-20.63	-20.2 ± 0.7	-0.99 ± 0.02	QFM
590 Ma-S	14ZA12D	-19.97	-20.51	-20.3 ± 0.3	-1.00 ± 0.01	QFM
570 Ma-W	14ZA01	-17.47	-19.09	-18.3 ± 0.8	+0.44 ± 0.07	NNO
570 Ma-E	14ZA23	-18.73	-20.67	-20.1 ± 1.0	-0.99 ± 0.03	QFM
560 Ma-S	14ZA10	-17.87	-19.11	-18.4 ± 0.6	+0.40 ± 0.05	NNO
560 Ma-N	14ZA18	-20.34	-20.79	-20.6 ± 0.2	-1.00 ± 0.01	QFM
560 Ma-N	14ZA19B	-19.63	-20.76	-20.2 ± 0.6	-0.99 ± 0.02	QFM
560 Ma-N	14ZA20B	-19.87	-20.71	-20.3 ± 0.4	-1.00 ± 0.02	QFM
560 Ma-N	14ZA21B	-19.69	-20.67	-20.3 ± 0.5	-1.00 ± 0.02	QFM
550 Ma Ngoura	NA01	-17.45	-18.69	-18.1 ± 0.6	+0.32 ± 0.05	NNO
550 Ma Ngoura	NA03	-17.38	-18.41	-17.9 ± 0.5	+0.31 ± 0.04	NNO
550 Ma Ngoura	NA06	-17.79	-18.96	-18.4 ± 0.6	+0.34 ± 0.04	NNO
550 Ma Moyto 2	NA18	-19.50	-20.47	-20.2 ± 0.5	-1.00 ± 0.02	QFM

Average = average values of the logfO₂ and ΔQFM including the uncertainty in the averages.

(Supplementary Table S1; Boehnke et al., 2013). The low T_{Zr}(°C) temperatures are consistent with the inheritance-rich granites described by Miller et al. (2003). It is postulated that inheritance-rich granites require infiltration of water-rich fluids that could be derived by dehydration of crust in the zone of melting. The granites from Guéra Massif and Lake Fitri are known to contain a significant amount of inherited zircons, and partial melting (~800–720°C) and fractional crystallization models (~910–740°C) of the collisional (e.g., 595–590 Ma rocks Guéra Massif) and post-collisional (e.g., Lake Fitri) systems indicate that water-saturated or near water-saturated conditions yield the best results (Shellnutt et al., 2017, 2018, 2019a). Consequently, it is possible that some of the low biotite temperature estimates are not necessarily due to sub-solidus re-equilibration during metamorphism or hydrothermal alteration (Ackerson et al., 2018). Indeed, the biotite and whole rock

T_{Zr}(°C) temperature estimates in this study lend support to this conclusion and they were likely derived from inheritance- and water-rich parental magmas. The reason for the secular temperature change is uncertain, although the biotites from the 595 Ma rocks have the highest temperatures, the host rock does not contain amphibole whereas the lower temperatures biotites are found in rocks with amphibole. Therefore, it is possible that the low biotite temperature estimates may be due to their later crystallization (i.e., post amphibole).

The oxygen fugacity of the investigated granites does not show a secular trend but the granite bodies in the northern portion of the Guéra Massif around Mongo tend to be oxidizing whereas those to the east and south are reducing. The only exception is samples 14ZA10 (560 Ma-S) which is relatively oxidizing. A similar relationship is observed in the Lake Fitri granites where the Ngoura granites are oxidizing



and the Moyto granites are reducing. In general, the biotites that have low Ti content also have low fO_2 estimates. The concentration of ferrous iron usually varies among different sample suites that differ in redox conditions, and the oxidation

state of magma activity controls the extent of Fe²⁺-enrichment in the magma sequence during its evolution (e.g., Larsen, 1976). In this case, the biotite of 590 Ma-S, 570 Ma-E, and 560 Ma-N plutons are more enriched in Fe²⁺ which

is associated with relatively reducing magmatic conditions; the Fe^{2+} -poor biotites of 595 Ma, 590 Ma-N, 570 Ma-W, and 560 Ma-S plutons are associated with relatively oxidizing magmatic conditions.

High f_{O_2} magmatic systems usually crystallize Fe-Ti oxide minerals such as ilmenite, hematite, and magnetite and that the appearance of hematite indicates the culmination in oxidation state in felsic rocks (Lindsley, 1991). The petrography and scanning electron microscopy investigation of this study did not identify primary hematite and the rocks have the extremely low abundance of ilmenite and magnetite which are primarily observed as inclusions within biotite or amphibole. The concentration of SiO_2 in the collisional granites is variable (59.7–74.8 wt%), whereas the post-collisional granites (69.3–76.9 wt%) is less variable but both can be very high (Pham, 2018; Shellnutt et al., 2018), which may be the reason for the low abundance of Fe-Ti oxide minerals.

The change in estimated pressure of the biotites from Guéra Massif generally shows a flat to slightly decreasing trend from oldest to youngest rocks (Figure 7D), possibly reflecting a decline of pressure associated with the tectonic transition from compressional to extensional stress. Our results show that there is significant pressure variation for some plutons. The 560 and 590 Ma-S plutons have higher biotite pressure estimates (0.27 ± 0.05 , 0.25 ± 0.09 GPa) compared to the 560 Ma-N (0.14 ± 0.07 – 0.19 ± 0.03 GPa) and 590 Ma-N (0.13 ± 0.02 GPa) granites. The barometric dichotomy could be due to a pressure gradient in the 560 and 590 Ma plutons related to their location within the magma body as it was emplaced. In other words, the exhumed southern regions of the plutons correspond to the base of the intrusions whereas the northern region represents the upper portions of the pluton. However, the amphibole pressure estimates from the northern portions of the 590 and 560 Ma plutons are significantly different than the biotite estimates (Figures 7C,D). The higher amphibole (590 Ma-N = 0.50 ± 0.07 GPa; 560 Ma-N = 0.29 ± 0.15 – 0.39 ± 0.06 GPa) and lower biotite (590 Ma-N = 0.13 ± 0.02 GPa; 560 Ma-N = 0.14 ± 0.07 – 0.19 ± 0.03 GPa) pressure estimates are in contrast to the estimates from the southern portion of the 590 Ma pluton which have similar values ($P_{\text{Am}} = 0.20 \pm 0.15$ GPa; $P_{\text{Bt}} = 0.25 \pm 0.09$ GPa). A possible explanation for the pressure difference is that the amphibole is older and initially crystallized at higher pressure and was subsequently redistributed before magma consolidation after reaching neutral buoyancy in the crust (lower pressure). Consistent with this interpretation is the fact that the high pressure amphibole has higher TiO_2 , Al_2O_3 , CaO , Na_2O , and K_2O and lower FeO^t than the low pressure amphibole suggesting that it probably crystallized before significant feldspar crystallization occurred.

Tectonomagmatic Evolution of Guéra Massif Granites

Biotite composition can be used to determine the tectonic environment of host rocks (Abdel-Rahman, 1994; Shabani et al., 2003; Machev et al., 2004; Bónová et al., 2010; Kumar

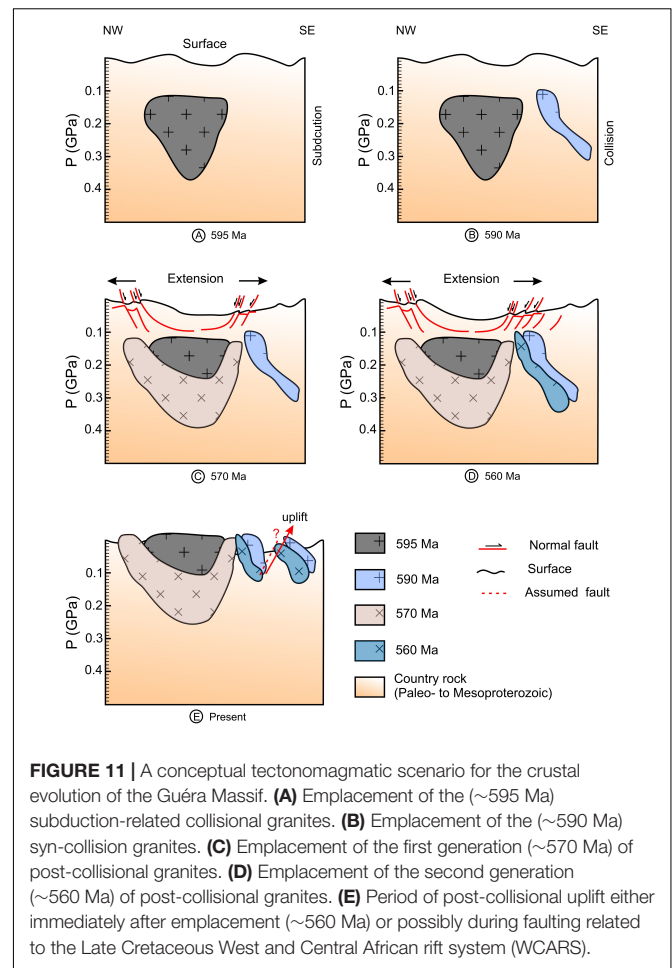


FIGURE 11 | A conceptual tectonomagmatic scenario for the crustal evolution of the Guéra Massif. **(A)** Emplacement of the (~595 Ma) subduction-related collisional granites. **(B)** Emplacement of the (~590 Ma) syn-collision granites. **(C)** Emplacement of the first generation (~570 Ma) of post-collisional granites. **(D)** Emplacement of the second generation (~560 Ma) of post-collisional granites. **(E)** Period of post-collisional uplift either immediately after emplacement (~560 Ma) or possibly during faulting related to the Late Cretaceous West and Central African rift system (WCARS).

and Pathak, 2010; Zhang et al., 2016). In this study we use the biotite tectonomagmatic characterization of Abdel-Rahman (1994) and Shabani et al. (2003). The older (595 Ma) collisional granites classify as calc-alkaline orogenic suites, and strongly contaminated and reduced (SCR) I-type granite (Figures 9A, 10A). In comparison, the younger (590 Ma) collisional granite is similar to anorogenic granite (anorogenic alkaline suite) in the diagram of Abdel-Rahman (1994) but straddle the fields of A-type granite, I-type granite, and SCR I-type (590 Ma-N) of Shabani et al. (2003) (Figures 9A, 10A). Indeed, the older (595 Ma) pluton is compositionally characteristic of volcanic-arc granite and was likely derived from a subduction modified mantle wedge source (Shellnutt et al., 2019a). In contrast, the 590 Ma plutons are different as they appear to be similar rocks associated with post-collisional extensional settings rather than collisional settings. Moreover, they have significant Mesoproterozoic (~1.0–1.9 Ga) inherited zircons suggesting they are likely derived from the crust (Shellnutt et al., 2019a). The overlapping and transition of biotite compositions and magmatic conditions suggest the younger (590 Ma) collisional rocks were likely related to the terminal stages of collisional. In other words, the first generation of collisional granites was emplaced at 595 Ma and related to subduction of oceanic crust beneath the Saharan

Metacraton whereas the 590 Ma plutons are probably related to syn-collisional magmatism that occurred during continent-continent collision between the Congo-São Francisco Craton and the Saharan Metacraton (Shellnutt et al., 2017, 2019a).

Post-collisional granites tend to be difficult to classify as they are commonly derived by melting of diverse (i.e., juvenile and ancient) crustal sources (Pearce, 1996). The post-collisional granites from Guéra Massif and Lake Fitri fall mostly within the field of anorogenic granites (A-field) but many straddle the boundary with peraluminous (P-field) granites (Figure 9; Abdel-Rahman, 1994). In comparison, nearly all data fall within the fields of I-type or SCR I-type granite in the classification of Shabani et al. (2003) (Figure 10). The seemingly contradictory results between the classification schemes of Abdel-Rahman (1994) and Shabani et al. (2003) is consistent with classification of post-collisional granite as Pearce (1996) demonstrates that these rocks overlap between the fields of volcanic-arc and within-plate granites with respect to Rb, Y, and Nb concentrations (Figure 7A). The first period of post-collisional granitic magmatism occurred at ~570 Ma and is probably related to crustal relaxation after oblique collision and shearing between the Congo-São Francisco Craton and the Saharan Metacraton (Ferré et al., 2002; Toteu et al., 2004). The second period of post-collisional magmatism was likely emplaced after an episode of regional crustal shortening (Ferré et al., 2002; Toteu et al., 2004). The timing of exhumation and exposure is unknown as it could be related to faulting either immediately after emplacement or possibly related to fault movement associated with the Cretaceous Western and Central African rift system (Figure 11; Genik, 1992).

In comparison to the Guéra Massif post-collisional granites, the Lake Fitri granites are different. The Lake Fitri granites tend to overlap between the anorogenic alkaline suites (A-field) and the peraluminous suites (P-field) but more importantly the higher pressure estimates indicate that they crystallized at greater depth. It is known that the Lake Fitri granites are isotopically more depleted [$\epsilon_{\text{Nd}}(t)$ +1.3 to +2.9] than the Guéra Massif post-collisional granites [$\epsilon_{\text{Nd}}(t)$ < -1.2] and suggest different sources were involved in their origin (Pham, 2018; Shellnutt et al., 2018, 2019a). Therefore, we conclude that the two regions probably represent separate domains/terraces and indicate that the crust near Late Fitri rocks was thicker and more juvenile whereas crust of the Guéra Massif was likely thinner and more radiogenic.

CONCLUSION

This study reports the compositions of biotite and hornblende from granitic rocks of the Guéra Massif and estimates of their likely crystallization conditions. The results offer new insight into the regional tectonic setting as well. The main conclusions are as follows:

1. The amphibole and biotite compositions show a trend of increasing total iron and decreasing magnesium content with decreasing age.
2. The biotites from the collisional granites tend to have higher crystallization temperatures, and crystallization

pressure, and are derived from parental magmas that were relatively oxidizing with redox conditions between NNO and QFM buffers.

3. The biotites from the post-collisional granites tend to yield lower crystallization temperatures and pressures but have similar redox conditions as the collisional rocks.
4. The biotite from the post-collisional granites from the Lake Fitri region crystallized at moderate to low temperatures, at high pressure with redox conditions at or near the NNO to QFM buffers.
5. The older (595 Ma) collisional granites have biotite compositions similar to rocks from orogenic suites whereas the younger (590 Ma) collisional granites have biotite compositions similar to anorogenic suites.
6. All biotites from the post-collisional rocks are characteristic of anorogenic suites although the crystals from the Lake Fitri granites have more variability and straddle the boundary with the peraluminous suites.
7. The post-collisional granites from Lake Fitri region and Guéra Massif have different emplacement depths and source composition. Thus, the Lake Fitri granites are probably unrelated to the Guéra Massif and were emplaced within a separate terrane/domain of the Saharan Metacraton.

DATA AVAILABILITY STATEMENT

All datasets generated for this study are included in the article/Supplementary Material.

AUTHOR CONTRIBUTIONS

CP wrote the manuscript, created the figures, and processed the data. JS conceived of the study and assisted with the writing and interpretations. M-WY collected the samples. YI analyzed the samples and wrote the method details. All authors contributed to the manuscript, read, and approved the submitted version.

FUNDING

This project received support from Ministry of Science and Technology (Taiwan) through grant 107-2628-M-003-003-MY3 to JS.

ACKNOWLEDGMENTS

Scott Whattam is thanked for editorial handling.

SUPPLEMENTARY MATERIAL

The Supplementary Material for this article can be found online at: <https://www.frontiersin.org/articles/10.3389/feart.2020.00318/full#supplementary-material>

REFERENCES

- Abdel-Rahman, A. M. (1994). Nature of biotites from alkaline, calc-alkaline, and peraluminous magmas. *J. Petrol.* 35, 525–541. doi: 10.1093/petrology/35.2.525
- Abdelsalam, M. G., and Dawoud, A. S. (1991). The kabus ophiolite melange, sudan and its bearing on the western boundary of the nubian shield. *J. Geol. Soc. Lond.* 148, 83–92. doi: 10.1144/gsjgs.148.1.0083
- Abdelsalam, M. G., Liégeois, J.-P., and Stern, R. J. (2002). The saharan metacraton. *J. Afr. Earth Sci.* 34, 119–136. doi: 10.1016/s0899-5362(02)00013-1
- Abdelsalam, M. G., and Stern, R. J. (1996). Mapping precambrian structures in the sahara desert with SIR-C/X-SAR radar: the neoproterozoic kerat suture. *NE Sudan. J. Geophys. Res.* 101, 23063–23076. doi: 10.1029/96je01391
- Ackerson, M. R., Mysen, B. O., Tailby, N., and Watson, E. B. (2018). Low-temperature crystallization of granites and the implications for crustal magmatism. *Nature* 559, 94–97. doi: 10.1038/s41586-018-0264-2
- Anderson, D. J., Lindsley, D. H., and Davidson, P. M. (1993). QUILF: a PASCAL program to assess equilibria among Fe-Mg-Mn-Ti oxides, pyroxenes, olivine, and quartz. *Comput. Geosci.* 19, 1333–1350. doi: 10.1016/0098-3004(93)90033-2
- Ayati, F., Yavuz, F., Asadi, H. H., Richards, J. P., and Jourdan, F. (2013). Petrology and geochemistry of calc-alkaline volcanic and subvolcanic rocks, Dalli porphyry copper-gold deposit, Markazi, Province, Iran. *Int. Geol. Rev.* 55, 158–184. doi: 10.1080/00206814.2012.689640
- Black, R. (1992). *Mission Géologique au Tchad du 14 Janvier au 08 Février 1992*. Rapport inedit. N'Djamena: PNUD/DRGM, 15.
- Boehnke, P., Watson, E. B., Trail, D., Harrison, T. M., and Schmitt, A. K. (2013). Zircon saturation re-visited. *Chem. Geol.* 351, 324–334. doi: 10.1016/j.chemgeo.2013.05.028
- Bónová, K., Broska, I., and Petrik, I. (2010). Biotite from Èierna hora Mountains granitoids (Western Carpathians, Slovakia) and estimation of water contents in granitoid melts. *Geol. Carpath.* 61, 3–17. doi: 10.2478/v10096-009-0040-1
- Bora, S., and Kumar, S. (2015). Geochemistry of biotites and host granitoid plutons from the Proterozoic Mahakoshal Belt, central India tectonic zone: implication for nature and tectonic setting of magmatism. *Int. Geol. Rev.* 57, 1686–1706. doi: 10.1080/00206814.2015.1032372
- Botcharnikov, R. E., Koepke, J., Holtz, F., and McCammon, C. (2005). The effect of water activity on the oxidation and structural state of Fe in a ferro-basaltic melt. *Geochim. Cosmochim. Ac.* 69, 5071–5085. doi: 10.1016/j.gca.2005.04.023
- Buddington, A. F., and Lindsley, D. H. (1964). Iron-titanium oxide minerals and synthetic equivalents. *J. Petrol.* 5, 310–357. doi: 10.1093/petrology/5.2.310
- Burkhard, D. J. M. (1991). Temperature and redox path of biotite-bearing intrusives: a method of estimation applied to S- and I-type granites from Australia. *Earth Planet. Sci. Lett.* 104, 89–98. doi: 10.1016/0012-821x(91)90240-i
- Burkhard, D. J. M. (1993). Biotite crystallization temperatures and redox states in granitic rocks as an indicator for tectonic setting. *Geol. Mijnbouw* 71, 337–349.
- Carmichael, I. S. E. (1991). The redox state of basic and silicic magmas: a reflection of their source regions? *Contrib. Mineral. Petrol.* 106, 129–141. doi: 10.1007/bf00306429
- Challener, S. C., and Glazner, A. F. (2017). Igneous or metamorphic? Hornblende phenocrysts as greenschist facies reaction cells in the Half Dome granodiorite, California. *Am. Mineral.* 102, 436–444. doi: 10.2138/am-2017-5864
- Eugster, H. P., and Wones, D. R. (1962). Stability reactions of the ferruginous biotite, annite. *J. Petrol.* 3, 82–125. doi: 10.1093/petrology/3.1.82
- Ferré, E., Gleizes, G., and Caby, R. (2002). Obliquely convergent tectonics and granite emplacement in the Trans-Saharan belt of Eastern Nigeria: a synthesis. *Precambrian Res.* 114, 199–219. doi: 10.1016/s0301-9268(01)00226-1
- Foster, M. D. (1960). "Interpretation of the composition of trioctahedral micas," in *US Geological Survey Professional Paper 354-B*, (Washington: United States Government Printing Office), 49.
- Freiberg, R., Hecht, L., Cuney, M., and Morteani, G. (2001). Secondary Ca-Al silicates in plutonic rocks and implications for their cooling history. *Contrib. Mineral. Petrol.* 141, 415–429. doi: 10.1007/s004100100241
- Frost, B. R., Barnes, C. G., Collins, W. J., Arculus, R. J., Ellis, D. J., and Frost, C. D. (2001). A geochemical classification for granitic rocks. *J. Petrol.* 42, 2033–2048. doi: 10.1093/petrology/42.11.2033
- Genik, G. J. (1992). Regional framework, structural and petroleum aspects of rift basins in Niger, Chad and the Central African Republic (CAR). *Tectonophysics* 213, 169–185. doi: 10.1016/b978-0-444-89912-5.50036-3
- Ghent, E. D., Nicholls, J., Siminy, P. S., Sevigny, H. H., and Stout, M. Z. (1991). Hornblende Geobarometry of the Nelson Batholith, Southeastern British Columbia: tectonic implications. *Can. J. Earth Sci.* 28, 1982–1991. doi: 10.1139/e91-180
- Ghiorso, M. S., and Sack, O. (1991). Fe-Ti oxide geothermometry: thermodynamic formulation and the estimation of intensive variables in silicic magmas. *Contrib. Mineral. Petrol.* 108, 485–510. doi: 10.1007/bf00303452
- Glazner, A. F., and Johnson, B. R. (2013). Late crystallization of K-feldspar and the paradox of megacrystic granites. *Contrib. Mineral. Petrol.* 166, 777–779.
- Hammarstrom, J. M., and Zen, E. (1986). Aluminum in hornblende: an empirical igneous geo-barometer. *Am. Mineral.* 71, 1297–1313.
- Hecht, L. (1994). "The chemical composition of biotite as an indicator of magmatic fractionation and metasomatism in Sn-specialised granites of the Fichtelgebirge (NW Bohemian Massif, Germany)," in *Metallogeny of Collisional Orogens*, eds R. Seltmann, H. Kämpf, and P. Möller (Praha: Czech Geological Survey), 295–300.
- Henry, B., Liégeois, J.-P., Nouar, O., Derder, M. E. M., Bayou, B., Bruguier, O., et al. (2009). Repeated granitoid intrusions during the Neoproterozoic along the western boundary of the Saharan Metacraton, Eastern Hoggar, Tuareg shield, Algeria: an AMS and U-Pb zircon age study. *Tectonophysics* 474, 417–434. doi: 10.1016/j.tecto.2009.04.022
- Hollister, L. S., Grissom, G. C., Peters, E. K., Stowell, H. H., and Gisson, V. B. (1987). Confirmation of the empirical correlation of Al in hornblende with pressure of solidification of calc-alkaline plutons. *Am. Mineral.* 72, 231–239.
- Isseini, M., Hamit, A., and Aberamane, M. (2013). The tectonic and geological framework of the Mongo area, a segment of the Pan-African Guera Massif in Central Chad: evidences from field observations and remote sensing. *Rev. Sci. Tchad.* 1, 4–12.
- Jayasuriya, K. D., O'Neill, H. S. C., Berry, A., and Campbell, S. J. (2004). A Mössbauer study of the oxidation state of Fe in silicate melts. *Am. Mineral.* 89, 1597–1609. doi: 10.2138/am-2004-11-1203
- Johnson, C. M., and Rutherford, M. J. (1989). Experimental calibration of the aluminum-in-hornblende geobarometer with applicable to Long Valley Caldera (California) volcanic rocks. *Geology* 17, 837–841.
- Kilinc, A., Carmichael, I. S. E., Rivers, M. L., and Sack, R. O. (1983). The ferriferous ratio of natural silicate liquids equilibrated in air. *Contrib. Mineral. Petrol.* 83, 136–140. doi: 10.1007/bf00373086
- Klerck, J., and Deutsch, S. (1977). Resultats preliminaires obtenus par la methode Rb/Sr sur l'age des formations Precambriennes de la region d'Uweinat (Libye). *Musee R. l'Afr. Centrale. Départ. Géol. Minérale. Rapp. Ann.* 83–94.
- Kress, V. C., and Carmichael, I. S. E. (1991). The compressibility of silicate liquids containing Fe₂O₃ and the effect of composition, temperature, oxygen fugacity and pressure on their redox states. *Contrib. Mineral. Petrol.* 108, 82–92. doi: 10.1007/bf00307328
- Kumar, S., and Pathak, M. (2010). Mineralogy and geochemistry of biotites from Proterozoic granitoid of western Arunachal Himalaya: evidence of bimodal granitogeny and tectonic af?nity. *J. Geol. Soc., India* 75, 715–730. doi: 10.1007/s12594-010-0058-0
- Kusnir, I., and Moutaye, H. A. (1997). Ressources minérales du Tchad: une revue. *J. Afr. Earth Sci.* 24, 549–562. doi: 10.1016/s0899-5362(97)00080-8
- Kusnir, I., and Schneider, J.-L. (1995). *Géologie, Ressources Mineérales et Ressources en eau du Tchad*. N'Djaména: Centre national d'appui à la recherche, 1.
- Larsen, L. M. (1976). Clinopyroxenes and coexisting mafic minerals from the alkaline Ilímaussaq intrusion. South Greenland. *J. Petrol.* 17, 258–290. doi: 10.1093/petrology/17.2.258
- Li, X., Chi, G., Zhou, Y., Deng, T., and Zhang, J. (2017). Oxygen fugacity of Yanshanian granites in South China and implications for metallogeny. *Ore Geol. Rev.* 88, 690–701. doi: 10.1016/j.oregeorev.2017.02.002
- Liégeois, J.-P., Abdelsalam, M. G., Ennih, N., and Ouabadi, A. (2013). Metacraton: nature, genesis and behavior. *Gondwana Res.* 23, 220–237. doi: 10.1016/j.gr.2012.02.016
- Liégeois, J.-P., Black, R., Navez, J., and Latouche, L. (1994). Early and late pan-african orogenies in the air assembly of terranes (Tuareg Shield, Niger). *Precambrian Res.* 67, 59–88. doi: 10.1016/0301-9268(94)90005-1
- Liégeois, J.-P., Latouche, L., Boughrara, M., Navez, J., and Guiraud, M. (2003). The LATEA metacraton (Central Hoggar, Tuareg shield, Algeria): behaviour of

- an old passive margin during the Pan-African orogeny. *J. Afr. Earth Sci.* 37, 161–190. doi: 10.1016/j.jafrearsci.2003.05.004
- Lindsley, D. H. (1991). Oxide minerals: petrologic and magnetic significance. *Rev. Mineral.* 25, 1–509.
- Luhr, J. F., Carmichael, I. S. E., and Varekamp, J. C. (1984). The 1982 eruptions of El Chichon volcano, Chiapas, Mexico—Mineralogy petrology of the anhydrite bearing pumices. *J. Volcanol. Geoth. Res.* 23, 69–108. doi: 10.1016/0377-0273(84)90057-x
- Luth, W. C., Jahns, R. H., and Tuttle, O. F. (1964). The granite system at pressures of 4 to 10 kilobars. *J. Geophys. Res.* 69, 759–773. doi: 10.1029/jz069i004p00759
- Machev, P., Klain, L., and Hecht, L. (2004). Mineralogy and chemistry of biotites from the belogradchik pluton—some petrological implications for granitoid magmatism in northwest Bulgaria. *Bulg. Geol. Soc. Annu. Sci. Conf. Geol. abstract.* 48–50.
- Miller, C. F., McDowell, S. M., and Mapes, R. W. (2003). Hot and cold granites? Implications of zircon saturation temperatures and preservation of inheritance. *Geology* 31, 529–532.
- Nachit, H., Ibhi, A., Abia, E. H., and Ohoud, M. B. (2005). Discrimination between primary magmatic biotites, reequilibrated biotites and neofomed biotites. *CR Geosci.* 337, 1415–1420. doi: 10.1016/j.crte.2005.09.002
- Nachit, H., Razafimahefa, N., Stussi, J. M., and Carron, J. P. (1985). Composition chimique des biotite et typologie magmatique des granitoïdes. *CR Acad. Sci. II* 301, 813–818.
- Nenova, P. I. (1997). “Fe23”: a computer program for calculating the number of Fe²⁺ and Fe³⁺ ions in minerals. *Comput. Geosci.* 23, 215–219. doi: 10.1016/s0098-3004(97)85445-3
- Nkouandou, O. F., Bardintzeff, J. M., Mahamat, O., Mefire, A. F., and Ganwa, A. A. (2017). The dolerite dyke swarm of Mongo, Guéra Massif (Chad, Central Africa): geological setting, petrography, and geochemistry. *Open Geosci.* 9, 138–150.
- Ottoneo, G., Moretti, R., Marini, L., and Zuccolini, M. V. (2001). Oxidation state of iron in silicate glasses and melts: a thermochemical model. *Chem. Geol.* 174, 157–179. doi: 10.1016/s0009-2541(00)00314-4
- Pearce, J. A. (1996). Source and settings of granitic rocks. *Episodes* 19, 120–125. doi: 10.18814/epiugs/1996/v19i4/005
- Pham, T. N. H. (2018). *Timing and Petrogenesis of Collisional and Post-Collisional Rocks of Guéra Massif, Republic of Chad*. master's thesis, National Taiwan Normal University, Taipei, TW.
- Pin, C., and Poidevin, J. L. (1987). U-Pb zircon evidence for a Pan-African granulite facies metamorphism in the Central African Republic. A new interpretation of the high-grade series of the northern border of the Congo Craton. *Precambrian Res.* 36, 303–312. doi: 10.1016/0301-9268(87)90027-1
- Piwinski, A. J. (1968). Experimental studies of igneous rock series, central Sierra Nevada batholith. *California. J. Geol.* 76, 193–215.
- Poidevin, J. L. (1994). Boninite-like rocks from the Paleoproterozoic greenstone belt of Bogoin, Central African Republic: geochemistry and petrogenesis. *Precambrian Res.* 68, 97–113. doi: 10.1016/0301-9268(94)90067-1
- Schlüter, T. (2008). *Geological Atlas of Africa*. Berlin: Springer-Verlag.
- Schmidt, M. W. (1992). Amphibole composition in tonalite as a function of pressure: an experimental calibration of the Al-in-hornblende barometer. *Contrib. Mineral. Petrol.* 110, 304–310. doi: 10.1007/bf00310745
- Shabani, A. A. T., Lalonde, A. E., and Whalen, J. B. (2003). Composition of biotite from granitic rocks of the Canadian Appalachian orogen: a potential tectonomagmatic indicator? *Can. Mineral.* 41, 1381–1396. doi: 10.2113/gscanmin.41.6.1381
- Shang, C. K., Satir, M., Morteani, G., and Taubald, H. (2010). Zircon and titanite age evidence for coeval granitization and migmatization of the early Middle and early Late Proterozoic Saharan Metacraton; example from the central North Sudan basement. *J. Afr. Earth Sci.* 57, 492–524. doi: 10.1016/j.jafrearsci.2009.12.006
- Shellnutt, J. G., Pham, T. N. H., Denyszyn, S., Yeh, M.-W., and Lee, T.-Y. (2017). Timing of collisional and post-collisional Pan-African Orogeny silicic magmatism in south-central Chad. *Precambrian Res.* 301, 113–123. doi: 10.1016/j.precamres.2017.08.021
- Shellnutt, J. G., Yeh, M.-W., Lee, T.-Y., Iizuka, Y., Pham, N. H. T., and Yang, C.-C. (2018). The origin of late ediacaran post-collisional granites near the Chad Lineament, Saharan Metacraton, South-Central Chad. *Lithos* 304–307, 450–467. doi: 10.1016/j.lithos.2018.02.020
- Shellnutt, J. G., Pham, N. H. T., Yeh, M.-W., and Lee, T.-Y. (2019a). “Two series of Ediacaran collision-related granites in the Guéra Massif (Chad): tectonomagmatic constraints on the terminal collision of the eastern Central African Orogenic Belt,” in *Fall Meeting (No. V31D-0160)*, Washington, DC: American Geophysical Union.
- Shellnutt, J. G., Yeh, M.-W., Pham, N. H. T., and Lee, T.-Y. (2019b). Cryptic regional magmatism in the southern Saharan Metacraton at 580 Ma. *Precambrian Res.* 332:105398. doi: 10.1016/j.precamres.2019.105398
- Stern, R. J. (1994). Arc assembly and continental collision in the Neoproterozoic E African Orogen: implication for the consolidation of Gondwanaland. *Annu. Rev. Earth Pl. Sci.* 22, 319–351. doi: 10.1146/annurev.earth.22.050194.001535
- Stern, R. J., Kröner, A., Bender, R., Reischmann, T., and Dawoud, A. S. (1994). Precambrian basement around Wadi Halfa, Sudan: a new perspective on the evolution of the East Saharan Craton. *Geol. Rundsch.* 83, 564–577. doi: 10.1007/bf01083228
- Suayah, I. B., Miller, J. S., Miller, B. V., Bayer, T. M., and Rogers, J. W. (2006). Tectonic significance of Late Neoproterozoic granites from the Tibesti massif in southern Libya inferred from Sr and Nd isotopes and U-Pb zircon data. *J. Afr. Earth Sci.* 44, 561–570. doi: 10.1016/j.jafrearsci.2005.11.020
- Sultan, M., Tucker, R. D., El Alfy, Z., Attia, R., and Ragab, A. G. (1994). U-Pb (zircon) ages for the gneissic terrane west of the Nile, southern Egypt. *Geol. Rundsch.* 83, 514–522. doi: 10.1007/bf00194158
- Tindle, A. G., and Webb, P. C. (1990). Estimation of lithium contents in trioctahedral micas using microprobe data: applications to micas from granitic rocks. *Eur. J. Mineral.* 2, 595–610. doi: 10.1127/ejm/2/5/0595
- Tindle, A. G., and Webb, P. C. (1994). Probe-AMPH – a spreadsheet program to classify microprobe-derived amphibole analyses. *Comput. Geosci.* 20, 1201–1228. doi: 10.1016/0098-3004(94)90071-x
- Toteu, S. F., Fouateu, R. Y., Penaye, J., Tchakounte, J., Mouangue, A. C. S., Van Schumus, W. R., et al. (2006). U-Pb dating of plutonic rocks involved in the nappe tectonic in southern Cameroon: consequence for the Pan-African orogenic evolution of the central African fold belt. *J. Afr. Earth Sci.* 44, 479–493. doi: 10.1016/j.jafrearsci.2005.11.015
- Toteu, S. F., Penaye, J., and Djomani, Y. H. P. (2004). Geodynamic evolution of the Pan-African belt in central Africa with special reference to Cameroon. *Can. J. Earth Sci.* 41, 73–85. doi: 10.1139/e03-079
- Tuttle, O. F., and Bowen, N. L. (1958). *Origin of Granite in the Light of Experimental of Studies in the System NaAlSi₃O₈-KAlSi₃O₈-SiO₂-H₂O*. Boulder, CO: Geological Society of America.
- Uchida, E., Endo, S., and Makino, M. (2007). Relationship between solidification depth of granitic rocks and formation of hydrothermal ore deposits. *Resour. Geol.* 57, 47–56. doi: 10.1111/j.1751-3928.2006.00004.x
- Wones, D., and Eugster, H. (1965). Stability of biotite: experiment, theory, and application. *Am. Mineral.* 50, 1228–1272.
- Wones, D. R. (1981). Mafic silicates as indicators of intensive variables in granitic magmas. *Min. Geol.* 31, 191–212.
- Yavuz, F. (2003a). Evaluating micas in petrologic and metallogenic aspect: I—definitions and structure of the computer program MICA+. *Comput. Geosci.* 29, 1203–1213. doi: 10.1016/s0098-3004(03)00142-0
- Yavuz, F. (2003b). Evaluating micas in petrologic and metallogenic aspect: Part II—Applications using the computer program Mica+. *Comput. Geosci.* 29, 1215–1228. doi: 10.1016/s0098-3004(03)00143-2
- Zen, E. (1988). Plumbing the depths of batholiths. *Am. J. Sci.* 289, 1137–1157. doi: 10.2475/ajs.289.10.1137
- Zhang, W., Lentz, D. R., Thorne, K. G., and McFarlane, C. (2016). Geochemical characteristics of biotite from intrusive felsic rocks around the Sisson Brook W-Mo-Cu deposit, west-central New Brunswick: an indicator of halogen and oxygen fugacity of magmatic systems. *Ore Geol. Rev.* 77, 82–96. doi: 10.1016/j.oregeorev.2016.02.004

Conflict of Interest: The authors declare that the research was conducted in the absence of any commercial or financial relationships that could be construed as a potential conflict of interest.

Copyright © 2020 Pham, Shellnutt, Yeh and Iizuka. This is an open-access article distributed under the terms of the Creative Commons Attribution License (CC BY). The use, distribution or reproduction in other forums is permitted, provided the original author(s) and the copyright owner(s) are credited and that the original publication in this journal is cited, in accordance with accepted academic practice. No use, distribution or reproduction is permitted which does not comply with these terms.